Bifurcations and monodromy of the axially symmetric 1:1:-2 resonance

Efstathiou, Konstantinos; Hanssmann, Heinz; Marchesiello, Antonella

Published in:
Journal of geometry and physics

DOI:
10.1016/j.geomphys.2019.103493

Publication date:
2019

Journal of Geometry and Physics 146 (2019) 103493

Contents lists available at ScienceDirect

Journal of Geometry and Physics

journal homepage: www.elsevier.com/locate/geomphys

Bifurcations and monodromy of the axially symmetric 1:1:−2 resonance

Konstantinos Efstathiou [a,*], Heinz Hanßmann [b], Antonella Marchesiello [c]

[a] Bernoulli Institute, University of Groningen, PO Box 407, 9700 AK Groningen, The Netherlands
[b] Mathematisch Instituut, Universiteit Utrecht, Postbus 80010, 3508 TA Utrecht, The Netherlands
[c] Department of Applied Mathematics, Faculty of Information Technology, Czech Technical University in Prague, Thákurova 9, 160 00 Prague 6, Czech Republic

ARTICLE INFO

Article history:
Received 2 June 2019
Received in revised form 2 August 2019
Accepted 16 August 2019
Available online 21 August 2019

Keywords:
Resonance
Bifurcations
Hamiltonian monodromy
Reduction

ABSTRACT

We consider integrable Hamiltonian systems in three degrees of freedom near an elliptic equilibrium in 1:1:−2 resonance. The integrability originates from averaging along the periodic motion of the quadratic part and an imposed rotational symmetry about the vertical axis. Introducing a detuning parameter we find a rich bifurcation diagram, containing three parabolas of Hamiltonian Hopf bifurcations that join at the origin. We describe the monodromy of the resulting ramified 3-torus bundle as variation of the detuning parameter lets the system pass through 1:1:−2 resonance.

1. Introduction

Let H^γ be a family of Hamiltonian systems in three degrees of freedom depending on parameters $\gamma \in \mathbb{R}^k$ and defined on $\mathbb{R}^6$ with canonical co-ordinates x_i, y_i, $i = 1, 2, 3$. We are interested in the dynamics near the elliptic equilibria, which are isolated for fixed γ. Moving the equilibrium to the origin we expand

$$H^\gamma(x, y) \;=\; \alpha_1(\gamma)I_1 \;+\; \alpha_2(\gamma)I_2 \;+\; \alpha_3(\gamma)I_3 \;+\; h.o.t. \tag{1}$$

where $I_i = \frac{1}{2}(y_i^2 + x_i^2)$, $i = 1, 2, 3$. The dynamical behaviour near the origin now depends on number-theoretic properties of the frequencies $\alpha_i = \alpha_i(\gamma)$. In the non-resonant case, where there are no integer relations

$$k_1\alpha_1 \;+\; k_2\alpha_2 \;+\; k_3\alpha_3 \;=\; 0 \tag{2}$$

among the frequencies, the normal form truncated at order 4 reads as

$$H(I) \;=\; \sum_{i=1}^{3} \alpha_i I_i \;+\; \sum_{i,j=1}^{3} \alpha_{ij} I_i I_j \;, \tag{3}$$

see [2,23] and references therein, and generically satisfies Kolmogorov's non-degeneracy condition

$$\det(\alpha_{ij})_{ij} \;\neq\; 0 \;.$$

The integrable Hamiltonian function (3) defines a ramified torus bundle with regular fibres $\mathbb{T}^3$, singular fibres $\mathbb{T}^2$ parametrised by the planes $I_i = 0$, $i = 1, 2, 3$, periodic orbits (the normal modes, also singular fibres of the ramified torus bundle) parametrised by the I_i-axes and the equilibrium (giving the most singular fibre of the ramified torus bundle) at

* Corresponding author.
E-mail address: konstantinos@efstathiou.gr (K. Efstathiou).

https://doi.org/10.1016/j.geomphys.2019.103493
0393-0440/

the origin $I_1 = I_2 = I_3 = 0$; all this is also valid in the indefinite case (where the frequencies α_i do not all have the same sign). Kolmogorov's non-degeneracy condition allows to apply KAM theory [2] whence the original Hamiltonian (1) defines a Cantorised ramified torus bundle, with fibres $\mathbb{T}^n$, $n = 2, 3$ parametrised by Cantor sets — obtained from their smooth counterparts above by strong non-resonance conditions (e.g. Diophantine conditions) on the internal frequencies of the tori.

This description of the local dynamics of (1) remains correct in case of resonances if these are of order $|k| := |k_1|+|k_2|+|k_3| \geq 5$ since then the normal form truncated at order 4 is still given by (3). Thus, for an open and dense subset of parameters γ a substantial part of the dynamics near the origin is rather transparent. The elliptic equilibrium has three normal modes and the majority of bounded trajectories is quasi-periodic, with three Cantor sets of Hausdorff-dimension 2 organising the distribution of invariant tori. Note that in the positive definite case $\alpha_i > 0$, $i = 1, 2, 3$ (as well as in the negative definite case) the equilibrium is stable in the sense of Lyapunov, while indefinite elliptic equilibria are expected to be unstable due to Arnol'd diffusion.

In case of a single resonance (2) of order $|k| \leq 4$ the normal form truncated at order 4 is still integrable but contains extra 'resonant terms' of order $|k|$. The resulting ramified torus bundle and its Cantorised counterpart thus depend on the resonance at hand. For instance, an indefinite elliptic equilibrium with resonance $2\alpha_1 + \alpha_2 = 0$ may have (in three degrees of freedom) only two normal modes, see [3,9]. Single resonances (2) among the normal frequencies $\alpha_i = \alpha_i(\gamma)$ define hypersurfaces in the parameter space and detuning the frequencies shows how to pass from one open region to a neighbouring one.

In case of two independent resonances (2) the frequencies are integer multiples $\alpha_i = n_i\alpha$, $i = 1, 2, 3$ (with $\gcd(n_1, n_2, n_3) = 1$) of a basic frequency $\alpha \in \mathbb{R}$ and one speaks of the n_1:n_2:n_3 resonance

$$\text{Osc}(n_1{:}n_2{:}n_3): \qquad K = n_1I_1 + n_2I_2 + n_3I_3$$

(scaling time allows to achieve $\alpha = 1$). In this paper we study the indefinite 1:1:−2 resonance where (1) reads as

$$H^\gamma(x, y) = (\alpha + \delta_1(\gamma))I_1 + (\alpha + \delta_2(\gamma))I_2 - (2\alpha + \delta_3(\gamma))I_3 + h.o.t. \tag{4}$$

with detuning $\delta = \delta(\gamma)$; for the moment we refrain from scaling time to achieve $\alpha = 1$. Smooth changes of parameters $\gamma \mapsto \delta(\gamma)$ allow to skip the γ-dependence in (4) altogether and study H^δ instead. The Hamiltonians with a 1:1:−2 resonant equilibrium at the origin are thus given by $2\delta_1 = 2\delta_2 = \delta_3$.

Remark 1. We expect that the three 'resonant terms' of order 3 make the normal form truncated at order 3 non-integrable, similar to the (definite) 1:1:2 resonance for which non-integrability has been proven in the absence of extra symmetries [10]; see also [7] where the same result could be achieved for the 1:2:3 and 1:2:4 resonances.

To enforce integrability we impose an axial $\mathbb{S}^1$-symmetry of rotations about the x_3-axis. From Noether's theorem it follows that the third component

$$N = x_1y_2 - x_2y_1$$

of the angular momentum is an integral of motion. For an axially symmetric detuning we have $\delta_1 = \delta_2 =: \delta$ and subsume δ_3 into 2α. Adding the axially symmetric detuning βN of the 1:1 subresonance the Hamiltonian (4) becomes

$$H^\delta = \alpha L + \beta N + \delta R + h.o.t. \tag{5}$$

with

$$\text{Osc}(1{:}1{:}-2): \qquad L = I_1 + I_2 - 2I_3$$

and

$$\text{Osc}(1{:}1{:}0): \qquad R = I_1 + I_2.$$

Let H denote the normal form of H^δ with respect to L truncated at order 4. The conserved quantity N is inherited by H and the normalising procedure makes L an integral of motion as well. Since $\{N, L\} = 0$ the Hamiltonian H admits a $\mathbb{T}^2$-symmetry and the energy–momentum mapping

$$\mathcal{EM} := (N, L, H): \mathbb{R}^6 \longrightarrow \mathbb{R}^3 \tag{6}$$

turns $\mathbb{R}^6$ into a ramified torus bundle.

Remark 2. In the literature on integrable Hamiltonian systems, the diagram showing the set of regular and critical values of the energy–momentum mapping $\mathcal{EM}$ and the type of the corresponding fibres of $\mathcal{EM}$ is sometimes called the 'bifurcation diagram of $\mathcal{EM}$'. In this work, to avoid confusion we use the term *bifurcation diagram* only to refer to the set of (internal and external) parameter values for which the system undergoes a bifurcation and we use the term *set of critical values of* $\mathcal{EM}$ to refer to that 'bifurcation diagram of $\mathcal{EM}$'.

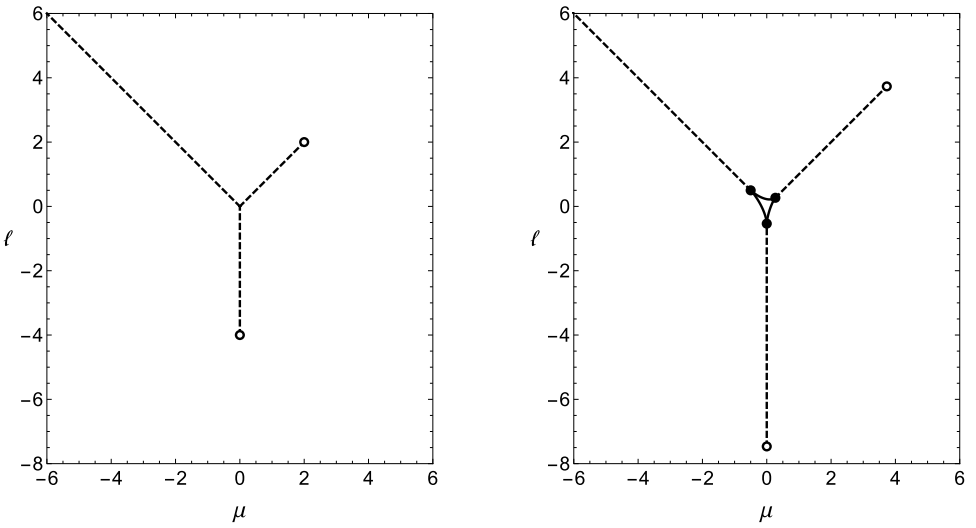

Fig. 1. The bifurcation diagram for a typical choice of normalised axially symmetric higher order terms in (5) showing two relevant phenomena: the effect of detuning near the origin and the termination of unstable normal modes at supercritical Hamiltonian Hopf bifurcations. Solid lines stand for quasi-periodic centre-saddle bifurcations while dashed lines stand for unstable periodic orbits which undergo Hamiltonian Hopf bifurcations at the bullets — subcritical at a solid bullet • and supercritical at an open bullet ∘. The left figure is without detuning ($\delta = 0$); here, the origin $(\mu, \ell) = (0, 0)$ stands for the 1:1:−2 resonant equilibrium and has three unstable normal modes. In the right figure $\delta \neq 0$ and the equilibrium has three stable normal modes that then undergo subcritical Hamiltonian Hopf bifurcations to become unstable.

After reduction of the $\mathbb{T}^2$-symmetry the values μ of N and ℓ of L serve as (internal) parameters. The set of critical values of the energy–momentum mapping (6) provides for a concise description of the dynamics defined by H. This set of critical values is in turn determined by the bifurcation diagram (in the (μ, ℓ)-plane) of the reduced system. In Fig. 1 we give two of the bifurcation diagrams we derive in Section 3 of the present paper. During the process it is instructive to include the detuning δ as (external) parameter, even if one were only interested in the case $\delta = 0$ of the 1:1:−2 resonance itself.

This paper is organised as follows. Before determining in Section 3 the general form of $\mathbb{T}^2$-symmetric higher order terms of (5) we pass in Section 2 to rotated co-ordinates that better reveal that not only L and R but also N is a resonant oscillator. Section 2 details the reduction of the $\mathbb{T}^2$-symmetry, i.e. the kinematics, while in Section 3 the one-degree-of-freedom dynamics is used to construct the bifurcation diagram. The set of critical values and the resulting monodromy (and their dependence on external parameters like δ) are discussed in Sections 4 and 5. The final Section 6 concludes the paper, coming back to the relation between (5) and its normal form truncated at order 4.

2. Kinematics

The axial symmetry ensures that the Hamiltonian (5) admits the three normal modes

$$(x_1(t), y_1(t)) \ , \ x_2 = -y_1, y_2 = x_1, x_3 = 0, y_3 = 0$$
$$(x_2(t), y_2(t)) \ , \ x_1 = -y_2, y_1 = x_2, x_3 = 0, y_3 = 0$$
$$(x_3(t), y_3(t)) \ , \ x_1 = 0, y_1 = 0, x_2 = 0, y_2 = 0.$$

The term normal mode is often restricted to periodic orbits where the remaining co-ordinates rest at 0 as in the normal 3-mode, instead of performing an 'enslaved' oscillation as in the normal 1- and 2-modes. To achieve the former for all normal modes we apply the orthogonal change of variables defined by

$$\begin{pmatrix} x_1 \\ x_2 \\ y_1 \\ y_2 \end{pmatrix} = \frac{1}{\sqrt{2}} \begin{pmatrix} 1 & 0 & 0 & -1 \\ 0 & 1 & -1 & 0 \\ 0 & 1 & 1 & 0 \\ 1 & 0 & 0 & 1 \end{pmatrix} \begin{pmatrix} q_1 \\ q_2 \\ p_1 \\ p_2 \end{pmatrix} \quad , \quad x_3 = q_3, y_3 = p_3, \tag{7}$$

which turns the symplectic structure $\mathrm{d}x \wedge \mathrm{d}y$ into $\mathrm{d}q \wedge \mathrm{d}p$. The transformation (7) leaves the form of L and R invariant while $N = x_1 y_2 - x_2 y_1$ is revealed to be the Hamiltonian

$$\mathrm{Osc}(1{:}-1{:}0): \qquad N = \frac{p_1^2 + q_1^2}{2} - \frac{p_2^2 + q_2^2}{2} \tag{8}$$

of three coupled oscillators in 1:−1:0 resonance. An advantage of this point of view is that adding oscillators $\mathrm{Osc}(m_1{:}m_2{:}m_3)$ and $\mathrm{Osc}(n_1{:}n_2{:}n_3)$ yields again an oscillator $\mathrm{Osc}(m_1 + n_1{:}m_2 + n_2{:}m_3 + n_3)$.

Table 1
Non-trivial isotropy groups of the $\mathbb{T}^2$-action (14) and types of Φ-orbits.

Set	Elements	Isotropy subgroup	Φ-orbit	Dynamics
C_{123}	$z_1 = z_2 = z_3 = 0$	$\mathbb{T}^2$	Point	Equilibrium
C_{12}	$z_1 = z_2 = 0 \neq z_3$	$\{(s,t) \mid t = 0\} \cong \mathbb{T}^1$	$\mathbb{T}^1$	Normal 3-mode
C_{13}	$z_1 = z_3 = 0 \neq z_2$	$\{(s,t) \mid s = 0\} \cong \mathbb{T}^1$	$\mathbb{T}^1$	Normal 2-mode
C_{23}	$z_2 = z_3 = 0 \neq z_1$	$\{(s,t) \mid s+t = 0\} \cong \mathbb{T}^1$	$\mathbb{T}^1$	Normal 1-mode

Remark 3. Adding the multiple β of N in (5) yielded a detuning of the 1:1 resonant oscillators in the subspace $(x_3, y_3) = (q_3, p_3) = 0$ to frequencies $\alpha + \beta + \delta$ and $\alpha - \beta + \delta$ (next to -2α) without breaking the symmetry generated by N. Note that adding a multiple β of

$$\frac{x_1^2 + y_1^2}{2} - \frac{x_2^2 + y_2^2}{2} = -(q_1 p_2 - q_2 p_1)$$

or of

$$x_1 x_2 + y_1 y_2 = q_1 q_2 + p_1 p_2$$

would yield the same detuning, but at the price of breaking the symmetry generated by N. A general detuning of the 1:1 subresonance has indeed co-dimension three and would lead to all the phenomena detailed in [15] concerning higher order terms in the normal form.

2.1. Isotropy

Let $X_G : \dot{F} = \{F, G\}$ denote the Hamiltonian vector field defined by a function G and φ_t^G the corresponding flow. Identify $\mathbb{R}^6 \cong \mathbb{C}^3$ by introducing complex co-ordinates $z_j = p_j + \mathrm{i} q_j$, $j = 1, 2, 3$. The flow φ_t^N of X_N induces an $\mathbb{S}^1$-action on $\mathbb{C}^3$. For treating monodromy later on we prefer to have integer periodicities, so let us define

$$\mathbb{T}^1 := \mathbb{R}/\mathbb{Z}$$

(an $\mathbb{S}^1$ with radius $\frac{1}{2\pi}$) and use $z = (z_1, z_2, z_3)$ to write the $\mathbb{T}^1$-action induced by φ_t^N as

$$\begin{array}{rccc} \varphi^N : & \mathbb{T}^1 \times \mathbb{C}^3 & \longrightarrow & \mathbb{C}^3 \\ & (t, z) & \mapsto & \varphi^N_{2\pi t}(z) = (\mathrm{e}^{2\pi \mathrm{i} t} z_1,\ \mathrm{e}^{-2\pi \mathrm{i} t} z_2,\ z_3) \end{array} . \tag{10}$$

This action has trivial isotropy, except at $z_1 = z_2 = 0$ where the isotropy subgroup is $\mathbb{T}^1$. Similarly, the flow φ_t^L of X_L induces a $\mathbb{T}^1$-action on $\mathbb{C}^3$ given by

$$\begin{array}{rccc} \varphi^L : & \mathbb{T}^1 \times \mathbb{C}^3 & \longrightarrow & \mathbb{C}^3 \\ & (t, z) & \mapsto & \varphi^L_{2\pi t}(z) = (\mathrm{e}^{2\pi \mathrm{i} t} z_1,\ \mathrm{e}^{2\pi \mathrm{i} t} z_2,\ \mathrm{e}^{-4\pi \mathrm{i} t} z_3) \end{array} . \tag{11}$$

This action has non-trivial isotropies $\mathbb{Z}_2$ when $z_1 = z_2 = 0$ and $\mathbb{T}^1$ when $z_1 = z_2 = z_3 = 0$. Combining the two commuting $\mathbb{T}^1$-actions φ^N and φ^L one can define an action of $\mathbb{T}^2 = \mathbb{T}^1 \times \mathbb{T}^1$ on $\mathbb{C}^3$ given by

$$\begin{array}{ccc} \mathbb{T}^2 \times \mathbb{C}^3 & \longrightarrow & \mathbb{C}^3 \\ (s, t, z) & \mapsto & \varphi^L_{2\pi t} \circ \varphi^N_{2\pi s}(z) = (\mathrm{e}^{2\pi \mathrm{i}(s+t)} z_1,\ \mathrm{e}^{2\pi \mathrm{i}(t-s)} z_2,\ \mathrm{e}^{-4\pi \mathrm{i} t} z_3) \end{array} . \tag{12}$$

A direct computation shows that the $\mathbb{T}^2$-action (12) is not *effective* as the element $(s, t) = (\frac{1}{2}, \frac{1}{2}) \in \mathbb{T}^2$ acts as the identity on all of $\mathbb{C}^3$.

We need a pair of generators of $\mathbb{T}^1$-actions for which the combined $\mathbb{T}^2$-action is effective and coincides with (12) projected to $\mathbb{T}^2/(\frac{1}{2}, \frac{1}{2})$. Such a pair is given by N and J where the latter is defined as

$$\mathrm{Osc}(1{:}0{:}{-1}) : \quad J = \frac{1}{2}(N + L) . \tag{13}$$

The flows φ_s^N and φ_t^J on $\mathbb{R}^6$ combine to the effective $\mathbb{T}^2$-action

$$\begin{array}{rccc} \Phi : & \mathbb{T}^2 \times \mathbb{C}^3 & \longrightarrow & \mathbb{C}^3 \\ & (s, t, z) & \mapsto & (\mathrm{e}^{2\pi \mathrm{i}(s+t)} z_1,\ \mathrm{e}^{-2\pi \mathrm{i} s} z_2,\ \mathrm{e}^{-2\pi \mathrm{i} t} z_3) \end{array} \tag{14}$$

with momentum mapping $(N, J) : \mathbb{R}^6 \longrightarrow \mathbb{R}^2$. Table 1 summarises the isotropies of Φ and the topological types of the corresponding Φ-orbits.

Table 2
The Poisson bracket relations among the basic invariants.

$\{\downarrow,\rightarrow\}$	N	L	J	R	X	Y
N	0	0	0	0	0	0
L	0	0	0	0	0	0
J	0	0	0	0	0	0
R	0	0	0	0	$2Y$	$-2X$
X	0	0	0	$-2Y$	0	$N^2+2LR-3R^2$
Y	0	0	0	$2X$	$3R^2-2LR-N^2$	0

2.2. Reduction

The reduction of the $\mathbb{T}^2$-symmetry is best performed by using a Hilbert basis of the algebra of $\mathbb{T}^2$-invariant functions as variables on the reduced phase space, see [8]. As proven in [18,24] this algebra is generated by $\mathbb{T}^2$-invariant polynomials.

Proposition 4. *The algebra $\mathcal{A}$ of invariant polynomials of the action Φ in (14) is generated by the real polynomials N, J and R together with X and Y defined by*

$$\begin{aligned} X = \mathrm{Re}(z_1z_2z_3) &= p_1p_2p_3 - q_1q_2p_3 - q_1p_2q_3 - p_1q_2q_3 \ , \\ Y = \mathrm{Im}(z_1z_2z_3) &= q_1p_2p_3 + p_1q_2p_3 + p_1p_2q_3 - q_1q_2q_3 \ . \end{aligned}$$

These satisfy the syzygy

$$S(N,J,R,X,Y) \coloneqq X^2 + Y^2 - (R^2-N^2)(R+N-2J) = 0 \ , \tag{15}$$

together with the inequality $R \geq R_{\min} \coloneqq \max(|N|, 2J-N) \geq 0$. These relations define a semi-algebraic variety in $\mathbb{R}^5$.

Note that $(N,L) \mapsto (N,J)$ has the inverse $L = 2J - N$ whence it is also possible to use the generators N, L, R, X, Y of $\mathcal{A}$ which satisfy

$$S(N,L,R,X,Y) = X^2 + Y^2 - (R^2-N^2)(R-L) = 0 \tag{16}$$

and $R \geq R_{\min} = \max(|N|, L) \geq 0$. In what follows we switch between these two sets of generators of $\mathcal{A}$ depending on which description is the most convenient.

For the Poisson structure we only need the Poisson bracket relations given in Table 2. As expected, the symmetry generators N, L and J are Casimir functions and fixing their values to $2\iota = \mu + \ell$, where ι denotes the value of J, yields the semi-algebraic surface

$$\mathcal{P}_{\mu\ell} = \left\{ (R,X,Y) \in \mathbb{R}^3 \;\middle|\; R \geq R_{\min},\ S_{\mu\ell}(R,X,Y) = 0 \right\} \ , \tag{17}$$

with Poisson structure

$$\{f,g\} = \langle \nabla f \times \nabla g \mid \nabla S_{\mu\ell} \rangle \ ,$$

where

$$S_{\mu\ell}(R,X,Y) = X^2 + Y^2 - (R^2-\mu^2)(R-\ell) \ .$$

Any smooth (resp. polynomial) Hamiltonian function H on $\mathbb{R}^6$ that is invariant under the $\mathbb{T}^2$-action Φ can be expressed as a smooth (resp. polynomial) function of the generators of $\mathcal{A}$, see [18,24]. Alternatively, H gives rise to a function $H_{\mu\ell}$ on the reduced phase space $P_{\mu\ell}$.

The semi-algebraic variety $P_{\mu\ell}$ is a surface of revolution about the R-axis. The type of singularities of $P_{\mu\ell}$ is given by the following result and the different possibilities are depicted in Fig. 2.

Proposition 5. *The semi-algebraic variety $\mathcal{P}_{\mu\ell}$ given by (17) is smooth everywhere except possibly at its 'tip' point $(R,X,Y) = (R_{\min},0,0)$. The latter point is a cusp (or cuspidal singularity of order 3) when $\mu = \ell = 0$; a cone (or conical singularity) when $\ell = |\mu| > 0$ or $\mu = 0$, $\ell < 0$; and smooth in all other cases.*

Proof. Since the semi-algebraic variety $\mathcal{P}_{\mu\ell}$ is a surface of revolution it is sufficient to consider its section with the plane $\{Y = 0\}$. Then we have

$$X^2 = (R^2-\mu^2)(R-\ell) \ , \quad R \geq R_{\min} = \max(|\mu|, \ell) \geq 0 \ .$$

Let $a_1 \geq a_2 \geq a_3$ denote the ordered values in the set $\{\mu, -\mu, \ell\}$ and write

$$X^2 = (R-a_1)(R-a_2)(R-a_3) \ , \quad R \geq R_{\min} = a_1 \geq 0 \ . \tag{18}$$

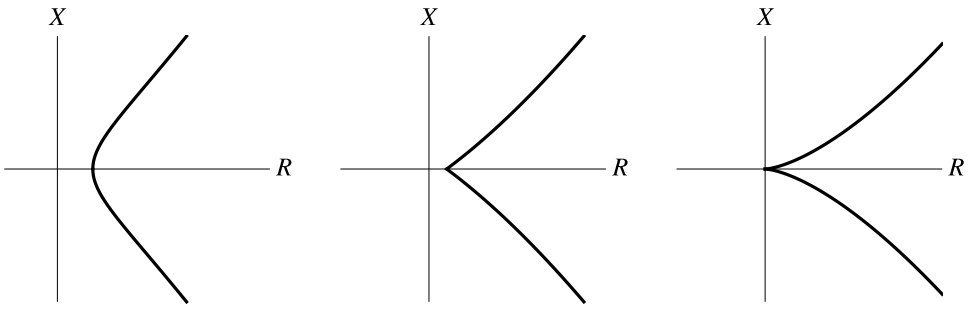

Fig. 2. The types of the singularities of the reduced spaces $\mathcal{P}_{\mu\ell}$ (which are surfaces of revolution about the R-axis). From left to right: smooth, conical and cuspidal.

The type of singularity at $R = a_1$ of $X^2 = f(R)$ with $f(a_1) = 0$ is determined by the lowest order term in the Taylor expansion of $f(R)$ at $R = a_1$. In particular, writing $X^2 = c(R-a_1)^k + h.o.t.$ we have a smooth curve when $k = 1$, a conical singularity when $k = 2$, and a cuspidal singularity when $k \geq 3$. Expand (18) in the form

$$X^2 \;=\; [(a_1-a_2)(a_1-a_3)](R-a_1) \;+\; [2a_1-a_2-a_3](R-a_1)^2 \;+\; (R-a_1)^3 \;.$$

The last expression shows that we have a cusp when $a_1 = a_2 = a_3$ implying $\mu = \ell = 0$. We have a cone when $a_1 = a_2 > a_3$ and one can check that this gives the cases $\ell = |\mu| > 0$ and $\mu = 0$, $\ell < 0$. The other cases lead to a smooth point. □

In particular, there are three open regions in the (μ, ℓ)-plane, each region being characterised by the (positive) value of $R_{\min}$, that is,

$$R_{\min} \;=\; \mu \;>\; \max(-\mu, \ell) \quad \text{or} \quad R_{\min} \;=\; -\mu \;>\; \max(\mu, \ell) \quad \text{or} \quad R_{\min} \;=\; \ell \;>\; |\mu| \;.$$

The three regions are separated by three half lines satisfying $\mu = \pm\ell$ or $\mu = 0$. Along these lines the tip is a cone while at $\mu = \ell = 0$ the tip is a cusp. The three half lines and their common limit point parametrising singular tips are the images under the momentum mapping (N, L) of the sets C_{23}, C_{13}, C_{12}, C_{123} in Table 1 with non-trivial isotropies $\mathbb{T}^1$ and $\mathbb{T}^2$ of the action Φ. After reconstruction to three degrees of freedom these are the elliptic equilibrium at the origin and its three normal modes.

3. Dynamics

The most general $\mathbb{T}^2$-symmetric higher order terms in (5) are functions of N, L, R, X and Y. As in (3) we normalise to order 4 in the original variables. Then X and Y appear only linearly and a rotation in the (X, Y)-plane removes the Y-term, whence

$$\begin{aligned} H^{\delta}_{N,L}(R,X,Y) \;&=\; \alpha L \;+\; \beta N \;+\; \delta R \;+\; X \;+\; \frac{\kappa}{2}R^2 \\ &\quad +\; (\lambda_1 N + \lambda_2 L)R \;+\; \frac{\gamma_1}{2}N^2 + \gamma_2 NL + \frac{\gamma_3}{2}L^2 \end{aligned} \tag{19}$$

is the most general choice in orders 3 and 4. The coefficient 1 of X can be obtained scaling time or space. Fixing the values $N = \mu$ and $L = \ell$ of the Casimirs we omit the constant part $\alpha\ell + \beta\mu + \frac{1}{2}\gamma_1\mu^2 + \gamma_2\mu\ell + \frac{1}{2}\gamma_3\ell^2$ and abbreviate

$$\lambda \;:=\; \delta \;+\; \lambda_1\mu \;+\; \lambda_2\ell \tag{20}$$

to obtain the reduced Hamiltonian

$$\mathcal{H}_\lambda(R,X,Y) \;=\; X \;+\; \lambda R \;+\; \frac{\kappa}{2}R^2 \;, \tag{21}$$

whose energy level sets are the parabolic cylinders

$$\mathcal{H}_\lambda^{-1}(h) \;=\; \left\{ (R,X,Y) \in \mathbb{R}^3 \;\middle|\; \mathcal{H}_\lambda(R,X,Y) = h \right\} \;.$$

The intersections of these with the reduced phase space $\mathcal{P}_{\mu\ell} \subseteq \mathbb{R}^3$ yield the orbits of $\mathcal{H}_\lambda$. The values μ and ℓ of the Casimirs serve as internal (or distinguished) parameters. We have equilibria where the two surfaces touch and where $\mathcal{H}_\lambda^{-1}(h)$ contains a singular point of $\mathcal{P}_{\mu\ell}$. We fix $\kappa \neq 0$ and only vary λ as an external parameter.

Remark 6. The coefficient $\kappa \neq 0$ in (19) could be chosen as $\kappa = 1$ through the combined scaling

$$(\lambda, \mu, \ell, R, X, Y, H) \;\mapsto\; (\kappa^{-1}\lambda, \kappa^{-2}\mu, \kappa^{-2}\ell, \kappa^{-2}R, \kappa^{-3}X, \kappa^{-3}Y, \kappa^{-3}H) \tag{22}$$

of space and time (which leaves the coefficient of X equal to 1). However, the dynamical consequence is that the basic frequency (or common multiple) of the unperturbed 1:1:−2 resonant oscillator, the coefficient α of L in (19), gets scaled to $\kappa\alpha$ and can no longer be scaled to 1. We therefore refrain from scaling the coefficient of R in (19) to $\frac{1}{2}$ until (46) in Section 4. Note that for negative κ the scaling (22) involves a reflection (combined with a scaling) of the parameter λ and the quantities X, Y and H.

Our aim here is to determine the bifurcation diagram for the Hamiltonian $\mathcal{H}_\lambda$ in the parameter space (δ, μ, ℓ). The coefficients λ_1 and λ_2 are fixed at rather small values while the detuning δ (and hence λ) is allowed to vary. For fixed values of λ_1 and λ_2, equation (20) defines a diffeomorphism between (λ, μ, ℓ)-space and (δ, μ, ℓ)-space, allowing direct translation of our findings between these two parameter spaces.

3.1. Regular equilibria and their bifurcations

Regular equilibria occur at smooth points of $\mathcal{P}_{\mu\ell}$ touching the parabolic cylinders $\mathcal{H}_\lambda^{-1}(h)$. They correspond to invariant 2-tori in three degrees of freedom and their bifurcations are triggered by two of these equilibria, or (all) three, meeting. All tangent planes of the parabolic cylinder $\mathcal{H}_\lambda^{-1}(h)$ are parallel to the Y-axis while a tangent plane of the surface of revolution $\mathcal{P}_{\mu\ell}$ can be parallel to the Y-axis only at points (R, X, Y) with $Y = 0$. Thus, the two surfaces can only touch at points in the $(Y{=}0)$-plane and for this it is necessary and sufficient that the parabola

$$\mathcal{H}_\lambda^{-1}(h) \cap \{Y = 0\} \;:\quad X \;=\; X_1(R) \;=\; h \;-\; \lambda R \;-\; \frac{\kappa}{2}R^2 \tag{23}$$

has the same derivative $X' = X'(R)$ as the variety

$$\mathcal{P}_{\mu\ell} \cap \{Y = 0\} \;:\quad X^2 \;=\; X_2(R)^2 \;=\; (R^2 - \mu^2)(R - \ell)\;, \quad R \geq R_{\min} \tag{24}$$

where we choose

$$X_2(R) \;=\; \sqrt{(R^2 - \mu^2)(R - \ell)}$$

as the 'upper' side. Note that the value h of the energy can always be adjusted to ensure that the two derivatives become equal at a common point (R, X) if $R \geq R_{\min}$. To compute the value of R we equate the slope

$$X_1' \;=\; -\lambda \;-\; \kappa R \tag{25}$$

of (23) with the slope of the variety (24). Adjusting h to actually have a common point of (23) and (24) we can use (the square of)

$$2X_2X_2' \;=\; 3R^2 \;-\; 2\ell R \;-\; \mu^2 \tag{26}$$

to obtain $R = R(\mu, \ell; \lambda, \kappa)$ from

$$\begin{aligned} 0 \;&=\; (2X_2X_1')^2 \;-\; (2X_2X_2')^2 \\ &=\; 4(\kappa R + \lambda)^2(R - \ell)(R^2 - \mu^2) \;-\; (3R^2 - 2\ell R - \mu^2)^2\;. \end{aligned} \tag{27}$$

An alternative method of obtaining equation (27) that gives the equilibria of the system is to search for double roots of the polynomial $F(R) = X_1^2(R) - X_2^2(R)$, cf. equation (33). The polynomial $F(R)$ is used in Section 3.3 to compute the bifurcations in the system, see Lemma 10.

Proposition 7. *Equation (27) has at most three solutions in the interval* $[R_{\min}, \infty[$. *There can be either one or three distinct solutions and in both cases the number of elliptic equilibria (centres) exceeds the number of hyperbolic equilibria (saddles) by* 1.

Proof. Let $S(R)$ denote the fifth order polynomial in R appearing in (27). Consider the root $R_* = \frac{1}{3}(\ell - (\ell^2 + 3\mu^2)^{1/2})$ of the polynomial $3R^2 - 2\ell R - \mu^2$ in (26). Then one checks that $R_* \leq R_{\min}$ and $S(R_*) \geq 0$ while $S(R_{\min}) \leq 0$. This implies that S must have at least two real roots in $]-\infty, R_{\min}[$, so it can have either 1 or 3 distinct real roots in $[R_{\min}, \infty[$.

Multiple roots are characterised by $S'(R) = 0$ whence distinct roots have $S'(R) \neq 0$ corresponding to elliptic equilibria if $S'(R) > 0$ and to hyperbolic equilibria if $S'(R) < 0$. The largest root of $S(R)$ must have $S'(R) > 0$ and is thus elliptic while the two smaller ones (if they exist and are distinct) alternate between hyperbolic and elliptic. □

Remark 8. The regular equilibria $(R, X, 0)$ of the reduced system yield invariant 2-tori in three degrees of freedom and it depends on the ratio between the internal frequencies

$$\frac{\partial H}{\partial N} \;=\; \beta \;-\; \alpha \;+\; (\gamma_1 - \gamma_2)\mu \;+\; (\gamma_2 - \gamma_3)\ell \;+\; (\lambda_1 - \lambda_2)R \tag{28a}$$

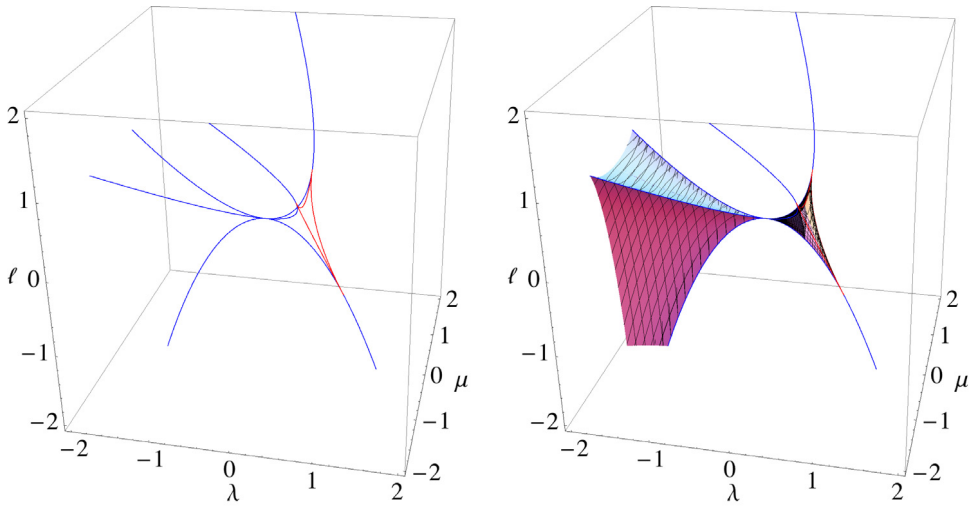

Fig. 3. Bifurcation set for $\kappa = 1$. (a) Hamiltonian Hopf bifurcations (blue curves) and cusp bifurcations (red curves). (b) Centre-saddle bifurcations are represented by the shown surfaces. The parts of the Hamiltonian Hopf bifurcation curves adjacent to centre-saddle bifurcations are subcritical Hamiltonian Hopf. The non-adjacent parts are supercritical. The transition takes place at the degenerate Hamiltonian Hopf bifurcations where the (red) cusp bifurcations emanate and the common point $(\lambda, \mu, \ell) = (0, 0, 0)$ of the three blue curves corresponds to the central equilibrium in 1:1:−2 resonance. (For interpretation of the references to colour in this figure legend, the reader is referred to the web version of this article.)

and

$$\frac{\partial H}{\partial J} \;=\; 2\,(\alpha \,+\, \gamma_2\mu \,+\, \gamma_3\ell \,+\, \lambda_2 R) \tag{28b}$$

(defined by the normal form $H = H^{\delta}_{NJ}$ obtained from (19) by replacing $L \mapsto 2J - N$) whether the resulting trajectories are periodic or quasi-periodic.

For a centre and a saddle to meet and vanish in a centre-saddle bifurcation the parabola (23) has to touch the variety (24) at an inflection point. This is decided by the derivative $X_1'' = -\kappa$ of (25) and the derivative

$$X_2 X_2'' \,+\, \left(X_2'\right)^2 \;=\; 3R \,-\, \ell \tag{29}$$

(of half) of (26). Equating the two derivatives or, equivalently, finding the triple roots of $F(R)$ gives a polynomial expression whose roots correspond to bifurcation points. In particular, we obtain the polynomial

$$\begin{aligned} 0 \;=\; & \kappa^4 R^4 \,+\, \kappa^2(4\lambda\kappa - 7)R^3 \,+\, 3(2\lambda^2\kappa^2 - 4\lambda\kappa + \kappa^2\ell + 3)R^2 \\ & + (4\lambda^3\kappa - 6\lambda^2 + \kappa^2\mu^2 + 4\lambda\kappa\ell - 6\ell)R \,+\, \lambda^4 \,-\, \kappa^2\mu^2\ell \,+\, 2\lambda^2\ell \,+\, \ell^2 \;. \end{aligned} \tag{30}$$

Inserting the solutions $R = R(\mu, \ell; \lambda, \kappa) \geq R_{\min}$ into (27) leads to three surfaces $\lambda = \lambda(\mu, \ell)$ of centre-saddle bifurcations $\mathbf{CS}_k$, $k = 1, 2, 3$ in parameter space (recall that we consider κ to be fixed).

This computation is done in Section 3.3 by finding the triple roots of the polynomial $F(R)$ in (33), see Lemma 10. Two surfaces parametrising centre-saddle bifurcations emanate from each of the three curves of subcritical Hamiltonian Hopf bifurcations $\mathbf{HH}_k^-$, $k = 1, 2, 3$ discussed in Section 3.2, see Fig. 3. In particular, the surface $\mathbf{CS}_1$ extends between $\mathbf{HH}_2^-$ and $\mathbf{HH}_3^-$, the surface $\mathbf{CS}_2$ extends between $\mathbf{HH}_1^-$ and $\mathbf{HH}_3^-$ and the surface $\mathbf{CS}_3$ extends between $\mathbf{HH}_1^-$ and $\mathbf{HH}_2^-$. Each surface $\mathbf{CS}_k$, $k = 1, 2, 3$ furthermore extends until a curve segment $\mathbf{CB}_k$ parametrising cusp bifurcations. A fourth surface $\mathbf{CS}_4$ of centre-saddle bifurcations has as boundary the union of the segments $\mathbf{CB}_k$, $k = 1, 2, 3$.

The non-degeneracy condition of a centre-saddle bifurcation requires that the derivative of (29) yields $X_2''' \neq 0$ (since the parabola (23) has zero third derivative). Looking for $X_2''' = 0$ we find $\kappa(\lambda + \kappa R) = 1$. The resulting

$$R \;=\; \frac{1}{\kappa^2} \,-\, \frac{\lambda}{\kappa} \tag{31}$$

yields at the singular points $R = 0$ and $R = \ell = |\mu|$ degenerate Hamiltonian Hopf bifurcations, see Sections 3.2 and 3.4. The theory in [19] predicts that two curves of cusp bifurcations emanate from each degenerate Hamiltonian Hopf bifurcation. The three degenerate Hamiltonian Hopf bifurcations form the vertices of a curvilinear triangle with the families $\mathbf{CB}_k$, $k = 1, 2, 3$, forming the corresponding edges. The cusp bifurcations are non-degenerate. Indeed, $X_2''' = 0$ turns the second derivative of (29) into $X_2 X_2^{(4)} + 3(X_2'')^2 = 0$ whence identifying X_2'' with $X_1'' \equiv -\kappa$ yields

$$X_2^{(4)} \;=\; \frac{-3\kappa^2}{X_2} \;\neq\; 0$$

and the sign – positive on the lower arc and negative on the upper arc, i.e. the same sign as the second derivative of $\mathcal{P}_{\mu\ell}$ with respect to Y – shows that this is the case of a cusp bifurcation governed by the singularity A_3^+, see [14]. Note that the surfaces defined by $R \geq R_{\min}$, (27), (30) and the exclusion of the cusp lines indeed parametrise centre-saddle bifurcations since the latter are given by exactly those parameter values where the non-degeneracy condition is not satisfied.

3.2. Hamiltonian Hopf bifurcations

A *singular* point $(R_{\min}, 0, 0)$ of $\mathcal{P}_{\mu\ell}$ (cone or cusp) is always an equilibrium. We get bifurcations when $\mathcal{H}_\lambda^{-1}(h^*)$, the parabolic surface given by

$$X \;=\; h^* \;-\; \lambda R \;-\; \frac{\kappa}{2}R^2 \tag{32}$$

(with $h^* = \lambda R_{\min} + \frac{1}{2}\kappa R_{\min}^2 = \lambda\ell + \frac{1}{2}\kappa\ell^2$ for $R_{\min} = \ell = \pm\mu$ and $h^* = 0$ for $R_{\min} = 0$), touches $\mathcal{P}_{\mu\ell}$ at the singular point, entering the singular point with a tangent line that coincides with that of the cone of $\mathcal{P}_{\mu\ell}$ (for the cusp this happens only when $\lambda = \mu = \ell = 0$, i.e. at the 1:1:−2 resonant equilibrium). Since the isotropy groups $\mathbb{T}^1$ are not discrete we expect these bifurcations to be Hamiltonian Hopf bifurcations. The type of intersection of $\mathcal{H}_\lambda^{-1}(h^*)$, given by (32), with $\mathcal{P}_{\mu\ell}$ separates stable equilibria $(R_{\min}, 0, 0)$ on $\mathcal{P}_{\mu\ell}$, where $\mathcal{H}_\lambda^{-1}(h^*)$ stays outside of $\mathcal{P}_{\mu\ell}$, from unstable equilibria, for which the intersection of $\mathcal{H}_\lambda^{-1}(h^*)$ with $\mathcal{P}_{\mu\ell}$ yields their stable=unstable manifolds in $\mathcal{P}_{\mu\ell}$. In three degrees of freedom these correspond to elliptic and hyperbolic periodic orbits; using the canonical equations of motion we immediately see that these Φ–orbits $\mathbb{T}^1$ indeed do not consist of equilibria (they form the three normal modes).

Correspondingly, for the supercritical type of the Hamiltonian Hopf bifurcation the touching parabolic surface $\mathcal{H}_\lambda^{-1}(h^*)$ stays outside of $\mathcal{P}_{\mu\ell}$ at the bifurcation parameter (and the bifurcating equilibrium is dynamically stable), while for the subcritical type $\mathcal{H}_\lambda^{-1}(h^*)$ yields the stable=unstable manifold of the bifurcating equilibrium (which is therefore dynamically unstable). The unstable periodic orbits resulting from the Hamiltonian Hopf bifurcations largely determine the monodromy of the system, discussed in Section 5.

Remark 9. Reducing only the $\mathbb{T}^1$-action (11) turns the normal modes into regular equilibria in two degrees of freedom that undergo Hamiltonian Hopf bifurcations. The Krein collision that triggers a Hamiltonian Hopf bifurcation and all other criteria [16] can be checked in one degree of freedom, but that the Krein collision does not occur at frequency 0 can only be verified in two degrees of freedom. However, the latter is merely needed for an approximate $\mathbb{T}^1$-symmetry that allows to reduce to one degree of freedom (after an additional normalisation) and in the present situation we already have imposed the $\mathbb{T}^1$-symmetry (10) as an exact symmetry. The whole bifurcation analysis thus takes place in one degree of freedom. Note that without imposing the $\mathbb{T}^1$-symmetry generated by N we would even have to check that a normal mode undergoing a Hamiltonian Hopf bifurcation does not have its internal frequency, the period, in (low order) normal-internal resonance with the normal frequencies at the Krein collision.

The analysis in Section 3.3 shows that there are three 1-parameter families of subcritical Hamiltonian Hopf bifurcations $\mathbf{HH}_k^-$, $k = 1, 2, 3$ that join with three 1-parameter families of supercritical Hamiltonian Hopf bifurcations $\mathbf{HH}_k^+$, $k = 1, 2, 3$; see Fig. 3. Their parametrisation is given in Proposition 11. As discussed in Section 3.1 there are two families of centre-saddle bifurcations emanating from each family of subcritical Hamiltonian Hopf bifurcations; the families of supercritical Hamiltonian Hopf bifurcations are isolated and meet the corresponding subcritical ones at three degenerate Hamiltonian Hopf bifurcations.

3.3. Bifurcation diagram for $\kappa \neq 0$

In this section we give a complete parametrisation of the bifurcation diagram (shown in Fig. 3) of the system passing through a 1:1:−2 resonance. As announced after having obtained equation (27) we consider the polynomial function

$$F(R) \;=\; X_1^2(R) \;-\; X_2^2(R) \;=\; \left(h - \lambda R - \frac{\kappa}{2}R^2\right)^2 \;-\; (R^2 - \mu^2)(R - \ell)\ . \tag{33}$$

Recall that $X_1(R)$ represents the energy level set $\mathcal{H}_\lambda^{-1}(h)$, see (23), while $X_2(R)$ and $-X_2(R)$ represent the upper and lower sides of $P_{\mu\ell} \cap \{Y = 0\}$ respectively, see (24). Then we have the following characterisation of the bifurcation set of the reduced Hamiltonian (21), which allows for a complete and uniform approach to parametrising the bifurcation set.

Lemma 10. *The set of parameter values $(h, \lambda, \kappa, \mu, \ell)$ for which (33) has a triple root $R = a$ (that is, $F(a) = F'(a) = F''(a) = 0$) with $a \geq R_{\min} = \max(|\mu|, \ell)$, describes the set of centre-saddle and Hamiltonian Hopf bifurcations. In particular, supercritical Hamiltonian Hopf bifurcations are characterised by $a = R_{\min}$ with $F'''(a) > 0$ and subcritical Hamiltonian Hopf bifurcations by $a = R_{\min}$ with $F'''(a) < 0$, while centre-saddle bifurcations are characterised by $a > R_{\min}$ with $F'''(a) \neq 0$. Quadruple roots $R = a > R_{\min}$, that is, moreover $F'''(a) = 0$ but $F^{(4)}(a) \neq 0$, correspond to cusp bifurcations and quadruple roots $R = a = R_{\min}$ correspond to degenerate Hamiltonian Hopf bifurcations.*

Proof. Suppose that $R = a$ is a triple root of $F(R)$. The relation $F(a) = 0$ gives $X_1(a) = \pm X_2(a)$. The '+ ' sign corresponds to a common point of the energy level set with the upper side of $P_{\mu\ell} \cap \{Y = 0\}$, the '−' sign with the lower side.

Subsequently $F'(a) = 0$ gives $X_1(a)X_1'(a) = X_2(a)X_2'(a)$. If $X_1(a) = X_2(a) = 0$ then the previous equation is satisfied. If $X_1(a) = \pm X_2(a) \neq 0$ then $X_1'(a) = \pm X_2'(a)$, implying that the energy level set touches the corresponding side of $P_{\mu\ell} \cap \{Y = 0\}$. Since we consider a triple root a of F the last implication $X_1'(a) = \pm X_2'(a)$ also follows if $X_1(a) = X_2(a) = 0$ since $F''(a) = 0$ gives

$$(X_1')^2(a) - (X_2')^2(a) + X_1(a)X_1''(a) - X_2(a)X_2''(a) = 0 \ . \tag{34}$$

As $X_2(a) = 0$ implies $a = R_{\min}$ the energy level set not only touches $P_{\mu\ell} \cap \{Y = 0\}$ at the point $(R_{\min}, 0)$ in this case, but furthermore the latter is singular, since for non-singular points we have $X_2'(R_{\min}) = \infty$. Dynamically this corresponds to a Hamiltonian Hopf bifurcation. Finally

$$F'''(R) = 2X_1(R)X_1'''(R) + 6X_1'(R)X_1''(R) - 2X_2(R)X_2'''(R) - 6X_2'(R)X_2''(R)$$

and for $a = R_{\min}$ we get

$$F'''(R_{\min}) = 6X_1'(R_{\min})X_1''(R_{\min}) - 6X_2'(R_{\min})X_2''(R_{\min}) \ .$$

If the Hamiltonian Hopf bifurcation takes place by a tangency at the upper side, then we find that $F'''(R_{\min}) > 0$ implies $X_1'' > X_2''$ so the level set $\mathcal{H}_\lambda^{-1}(h)$ touches from outside and we have a supercritical Hamiltonian Hopf bifurcation. If the tangency is with the lower side, then $X_1'' < -X_2''$ so the level set $\mathcal{H}_\lambda^{-1}(h)$ touches from outside and we again have a supercritical Hamiltonian Hopf bifurcation. Correspondingly, when $F'''(R_{\min}) < 0$ the level set $\mathcal{H}_\lambda^{-1}(h)$ touches from inside and the Hamiltonian Hopf bifurcation is subcritical. In between, when $F'''(R_{\min}) = 0$ (while $F^{(4)}(R_{\min}) \neq 0$) we have a degenerate Hamiltonian Hopf bifurcation (for more details on this see Section 3.4).

If $X_1(a) = \pm X_2(a) \neq 0$ then, as we have earlier seen, we also have $X_1'(a) = \pm X_2'(a)$, therefore from (34) we find $X_1''(a) = \pm X_2''(a)$. These conditions determine an inflection point between the two curves and therefore a centre-saddle bifurcation provided that $X_1'''(a) \neq \pm X_2'''(a)$. If the last non-degeneracy condition is not satisfied then we have a cusp bifurcation. This corresponds to $F'''(a) = 0$ (in addition to $F(a) = F'(a) = F''(a) = 0$) and $F^{(4)} = 6\kappa^2 \neq 0$. □

Given Lemma 10 we can compute the bifurcation diagram of the system by finding the triple roots of F that lie in $[R_{\min}, \infty[$.

Proposition 11. *The bifurcation diagram for $\kappa = 1$ consists of the 2-parameter families of centre-saddle bifurcations, the 1-parameter families of (non-degenerate) Hamiltonian Hopf and cusp bifurcations and the three degenerate Hamiltonian Hopf bifurcations given in Table 3.*

The proof of Proposition 11 is given in the Appendix, except for the degenerate Hamiltonian Hopf bifurcation which we treat in Section 3.4. The bifurcation set presented in Table 3 includes the centre-saddle and cusp bifurcations discussed in Section 3.1 and the Hamiltonian Hopf bifurcations discussed in Section 3.2. The bifurcation set in three-dimensional space (λ, μ, ℓ) is shown for $\kappa = 1$ in Fig. 3. Successive horizontal sections of constant ℓ are shown in Fig. 4. Recall that for $\kappa \neq 0$ we can scale invariants and parameters to obtain a system with $\kappa = 1$ and therefore the bifurcation diagram for any $\kappa \neq 0$ can be obtained by inverting the scaling.

3.4. The degenerate Hamiltonian Hopf bifurcation

Abbreviating

$$T = x_1y_2 - x_2y_1 \tag{35a}$$

$$U = \frac{x_1^2 + x_2^2}{2} \tag{35b}$$

$$V = \frac{y_1^2 + y_2^2}{2} \tag{35c}$$

$$W = x_1y_1 + x_2y_2 \tag{35d}$$

for a Hamiltonian system in two degrees of freedom, the standard form of the (non-degenerate) Hamiltonian Hopf bifurcation reads as

$$H_\nu = T + U + \nu V + aV^2 \ . \tag{36}$$

The non-degeneracy condition is $a \neq 0$ and the sign of a distinguishes between the supercritical case $a > 0$ and the subcritical case $a < 0$; see [20] for a proof. In the degenerate case $a = 0$ terms of order higher than four (in the original variables x, y) become important, see [4,5,19]. Indeed, if the coefficient b of V^3 is non-zero, then a C^∞-versal unfolding is given by

$$H_\nu = T + U + \nu_1 V + \frac{\nu_2}{2}V^2 + \nu_3 TV + bV^3 \ . \tag{37}$$

Table 3
Bifurcations for the 1:1:−2 resonant system in the case $\kappa = 1$. The quantities $\mu_\pm = \mu_\pm(a,\lambda)$ and $\ell_\pm = \ell_\pm(a,\lambda)$ are given in the (50) in Appendix, while $a_0(\lambda)$ is the unique non-negative root of the cubic polynomial $g(a)$ given in (56).

Type	Parametrisation of (λ, μ, ℓ)	Parameter ranges	Remarks
Centre-Saddle			
$\mathbf{CS}_1$	$(\lambda, -\mu_-(a,\lambda), \ell_-(a,\lambda))$	$\lambda < \frac{1}{2}$ and $0 < a < 1-\lambda-\sqrt{1-2\lambda}$ or $\frac{1}{2} < \lambda < 1$, $0 < a < 1-\lambda$	Extended by continuity to $\lambda = \frac{1}{2}$
$\mathbf{CS}_2$	$(\lambda, \mu_-(a,\lambda), \ell_-(a,\lambda))$	same as for $\mathbf{CS}_1$	
$\mathbf{CS}_3$	$(\lambda, \pm\mu_+(a,\lambda), \ell_+(a,\lambda))$	$\lambda < \frac{1}{2}$, $a_0(\lambda) < a < 1-\lambda-\sqrt{1-2\lambda}$	
$\mathbf{CS}_4$	$(\lambda, \pm\mu_-(a,\lambda), \ell_-(a,\lambda))$	$\frac{1}{2} < \lambda < 1$ and $1-\lambda < a < a_0(\lambda)$	
Cusp			
$\mathbf{CB}_1$	$(\lambda, -(\lambda-\sqrt{2\lambda-1}), 1-\lambda-\sqrt{2\lambda-1})$	$\frac{1}{2} < \lambda < 1$	$\partial\mathbf{CS}_1 \cap \partial\mathbf{CS}_4$
$\mathbf{CB}_2$	$(\lambda, \lambda-\sqrt{2\lambda-1}, 1-\lambda-\sqrt{2\lambda-1})$	$\frac{1}{2} < \lambda < 1$	$\partial\mathbf{CS}_2 \cap \partial\mathbf{CS}_4$
$\mathbf{CB}_3$	$(\frac{1}{2}, \mu, \frac{1}{4}+\mu^2)$	$\lambda \equiv \frac{1}{2}$, $-\frac{1}{2} < \mu < \frac{1}{2}$	$\partial\mathbf{CS}_3 \cap \partial\mathbf{CS}_4$
Hamiltonian Hopf (subcritical)			
$\mathbf{HH}_1^-$	$(\lambda, 1-\lambda-\sqrt{1-2\lambda}, 1-\lambda-\sqrt{1-2\lambda})$	$\lambda < \frac{1}{2}$	$\partial\mathbf{CS}_2 \cap \partial\mathbf{CS}_3$
$\mathbf{HH}_2^-$	$(\lambda, -(1-\lambda-\sqrt{1-2\lambda}), 1-\lambda-\sqrt{1-2\lambda})$	$\lambda < \frac{1}{2}$	$\partial\mathbf{CS}_1 \cap \partial\mathbf{CS}_3$
$\mathbf{HH}_3^-$	$(\lambda, 0, -\lambda^2)$	$\lambda < 1$	$\partial\mathbf{CS}_1 \cap \partial\mathbf{CS}_2$
Hamiltonian Hopf (supercritical)			
$\mathbf{HH}_1^+$	$(\lambda, 1-\lambda+\sqrt{1-2\lambda}, 1-\lambda+\sqrt{1-2\lambda})$	$\lambda < \frac{1}{2}$	
$\mathbf{HH}_2^+$	$(\lambda, -(1-\lambda+\sqrt{1-2\lambda}), 1-\lambda+\sqrt{1-2\lambda})$	$\lambda < \frac{1}{2}$	
$\mathbf{HH}_3^+$	$(\lambda, 0, -\lambda^2)$	$\lambda > 1$	
Hamiltonian Hopf (degenerate)			
$\mathbf{HH}_1^0$	$(\frac{1}{2}, \frac{1}{2}, \frac{1}{2})$	A single point	$\partial\mathbf{CB}_2 \cap \partial\mathbf{CB}_3$
$\mathbf{HH}_2^0$	$(\frac{1}{2}, -\frac{1}{2}, \frac{1}{2})$	A single point	$\partial\mathbf{CB}_1 \cap \partial\mathbf{CB}_3$
$\mathbf{HH}_3^0$	$(1, 0, -1)$	A single point	$\partial\mathbf{CB}_1 \cap \partial\mathbf{CB}_2$

As expected, the coefficient of V^2 has turned into the unfolding parameter ν_2, but furthermore a third unfolding parameter ν_3 has emerged, the coefficient of the fourth order term TV. This C^∞-modal parameter can be removed by passing to a C^0-versal unfolding, again see [4,5,19], subject to $\nu_3 \notin \{0, \pm\sqrt{-b}, \pm\sqrt{3b}\}$.

For a general Hamiltonian with an equilibrium $0 \in \mathbb{R}^4$ in 1:−1 resonance, the standard forms (36) and (37) have to be achieved through normalisation with respect to T (and U). In our application to (19) the Hamiltonian already is symmetric with respect to N, which amounts here to symmetry with respect to T. This allows to reduce to one degree of freedom and all other questions can be answered using the reduced system; see [14,16,17] for criteria concerning the supercritical and subcritical Hamiltonian Hopf bifurcations. To formulate similar criteria for the degenerate Hamiltonian Hopf bifurcation we therefore reduce (37) to one degree of freedom, using the invariants (35b)–(35d) of the S^1-action generated by (35a) as variables subject to the syzygy

$$2UV = \frac{W^2+T^2}{2}$$

and the inequalities $U \geq 0$, $V \geq 0$. Fixing $T = \theta$ this yields one sheet $\mathcal{P}_\theta$ of a 2-sheeted hyperboloid, a cone if $\theta = 0$, and the orbits of the flow defined by (37) are given by the intersections (within $\mathbb{R}^3 = \{U, V, W\}$) with the parabolic cylinders $\{H_\nu = h\}$, i.e. the latter sets are flat in the W-direction. Such parabolic cylinders can touch the reduced phase space $\mathcal{P}_\theta$ only within the plane $\{W = 0\}$, whence equilibria occur where the curves

$$U = 0 \tag{38a}$$

$$U = h - \theta - \nu_1 V - \frac{\nu_2}{2}V^2 - \nu_3 TV - bV^3 \tag{38b}$$

have the same derivative (adjusting the height h of (38b) appropriately). Note that this formulation lends itself for a straightforward generalisation to S^1-symmetric Hamiltonian Hopf bifurcations where none of the corresponding curves (38) is expected to be the co-ordinate axis, again compare with [14,16,17].

The point $V = 0$ corresponds to the singular tip $(U, V, W) = (0, 0, 0)$ of the cone, so it is always an equilibrium. It is where the Hamiltonian Hopf bifurcation takes place that (38a) and (38b) have the same derivative in $V = 0$, i.e. where the corresponding equilibrium in $\mathbb{R}^4$ has normal frequencies in 1:−1 resonance. This means that the difference function between (38b) and (38a) – which for the standard form (37) is simply (38b) – has a double root at the singular point of

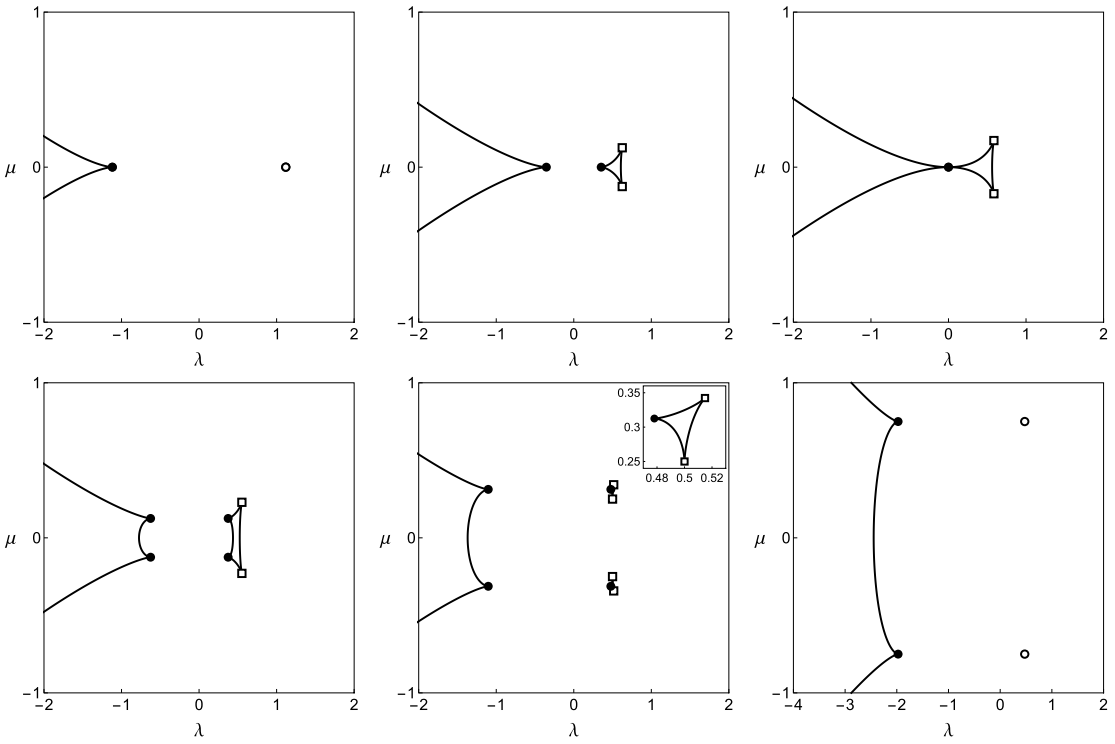

Fig. 4. Bifurcation curves for $\kappa = 1$ and fixed values of ℓ (horizontal slices of the three-dimensional bifurcation diagram in Fig. 3). From top left: $\ell = -5/4$, $\ell = -1/8$, $\ell = 0$, $\ell = 1/8$, $\ell = 5/16$, and $\ell = 3/4$. The • mark subcritical Hamiltonian Hopf bifurcations (for $\ell = 0$ the central equilibrium in 1:1:−2 resonance), the ∘ mark supercritical Hamiltonian Hopf bifurcations, and the □ mark cusp bifurcations. In the panel for $\ell = 5/16$ one of the smaller structures in the bifurcation diagram has been magnified in the inset.

the reduced phase space. Correspondingly, the first derivative of the difference function at $V = 0$ yields the first unfolding parameter ν_1. The second derivative then yields the second unfolding parameter ν_2, vanishing as well at the degenerate Hamiltonian Hopf bifurcation and otherwise distinguishing between the supercritical case (where the energy level set touches the cone from the outside) and the subcritical case (where $\{H_\nu = 0\}$ touches $\mathcal{P}_0$ from the inside). Note that the first derivative in fact yields $\nu_1 + \nu_3\theta$ from which we not only obtain the unfolding parameter ν_1 by taking $\theta = 0$, but also the modal parameter ν_3 by taking the derivative with respect to θ. Finally, the third derivative equals b and thus should be non-zero to have a 'non-degenerate' degenerate Hamiltonian Hopf bifurcation.

To check whether (and where) a degenerate Hamiltonian Hopf bifurcation takes place in the normal form (19) of the 1:1:−2 resonance we merely have to take derivatives of (the square root of) the curve (24) and of the curve (23) at $R = R_{\min} = \ell = |\mu| > 0$ and at $R = R_{\min} = \mu = 0$, $\ell < 0$. As already noted in (32), the value h of $\mathcal{H}_\lambda$ has to be adjusted to $h^* = \lambda\ell + \frac{1}{2}\kappa\ell^2$ or $h^* = 0$, respectively. Let us first concentrate on $R_{\min} = 0$. Then the cubic curve (24) becomes

$$X_2(R) \;=\; \pm R\sqrt{R-\ell} \tag{39}$$

with derivatives $X_2'(0) = \pm\sqrt{-\ell}$, $X_2''(0) = \pm\sqrt{-\ell}^{-1}$ and $X_2'''(0) = \mp\frac{3}{4}\sqrt{-\ell}^{-3}$, while (23) has derivatives $X_1'(0) = -\lambda$, $X_1''(0) = -\kappa$ and $X_1'''(0) = 0$. Equating the first derivatives yields

$$-\lambda \;=\; \pm\sqrt{-\ell}\ , \tag{40}$$

whence the parabola (23) touches the cubic (24) at the 'upper' side for $\lambda < 0$ and at the 'lower' side for $\lambda > 0$. Equating the second derivatives yields

$$-\kappa \;=\; \frac{\pm 1}{\sqrt{-\ell}}\ , \tag{41}$$

whence the Hamiltonian Hopf bifurcation is degenerate for

$$(\lambda, \mu, \ell) \;=\; (\frac{1}{\kappa}, 0, \frac{-1}{\kappa^2})\ .$$

For definiteness we restrict to a positive constant $\kappa > 0$, so the degenerate Hamiltonian Hopf bifurcation takes place at the 'lower' side of the cubic (24). We infer from (40) that $\frac{1}{\kappa} - \lambda$ can be used to unfold the Krein collision and from (20) that in

fact the detuning $\frac{1}{\kappa} - \delta$ plays the rôle of the unfolding parameter ν_1, while $-\lambda_1$ plays the rôle of the modal parameter ν_3. From (41) we conclude that the second derivative at $R = R_{\min} = 0$ of the difference function between (39) and (23) reads as

$$\frac{1}{\sqrt{-\ell}} - \kappa = \frac{\kappa^3}{2}(\ell + \frac{1}{\kappa^2}) + \frac{3\kappa^5}{8}(\ell + \frac{1}{\kappa^2})^2 + \cdots$$

whence the rôle of ν_2 is played by $\frac{1}{\kappa^2} + \ell$. The third derivative $\frac{3}{4}\kappa^3$ is positive for $\kappa > 0$ and in particular non-zero. Note that the latter also follows from $F^{(4)} \equiv 6\kappa^2 \neq 0$, see Eq. (33).

We now check the conditions at the other two possible values of $R_{\min}$. For both(!) $R_{\min} = \ell = \pm\mu > 0$ the cubic (24) becomes

$$X_2(R) = \pm(R - \ell)\sqrt{R + \ell} \tag{42}$$

with derivatives $X_2'(\ell) = \pm\sqrt{2\ell}$, $X_2''(\ell) = \pm\sqrt{2\ell}^{-1}$ and $X_2'''(\ell) = \mp\frac{3}{4}\sqrt{2\ell}^{-3}$, while $X_1'(\ell) = -\lambda - \kappa\ell$, $X_1''(\ell) = -\kappa$ and $X_1'''(\ell) = 0$. Equating the first derivatives yields

$$-\lambda - \kappa\ell = \pm\sqrt{2\ell}\ , \tag{43}$$

whence the parabola (23) touches the cubic (24) at the 'upper' side for $\lambda < -\kappa\ell$ and at the 'lower' side for $\lambda > -\kappa\ell$. Equating the second derivatives yields

$$-\kappa = \frac{\pm 1}{\sqrt{2\ell}}\ , \tag{44}$$

whence the Hamiltonian Hopf bifurcation is degenerate for

$$(\lambda, \mu, \ell) = (\frac{1}{2\kappa}, \frac{\pm 1}{2\kappa^2}, \frac{1}{2\kappa^2})\ .$$

Keeping $\kappa > 0$, the degenerate Hamiltonian Hopf bifurcation again takes place at the 'lower' side of the cubic (24). We infer from (43) that $\frac{1}{2\kappa} - \lambda$ can be used to unfold the Krein collision where (again) the detuning $\frac{1}{2\kappa} - \delta$ plays the rôle of the unfolding parameter ν_1, while $-\lambda_1$ plays the rôle of the modal parameter ν_3. From (44) we conclude that the second derivative at $R = R_{\min} = 0$ of the difference function between (42) and (23) reads as

$$\frac{1}{\sqrt{2\ell}} - \kappa = -\frac{\kappa^3}{2}(\ell - \frac{1}{2\kappa^2}) + \frac{3\kappa^5}{8}(\ell - \frac{1}{2\kappa^2})^2 + \cdots$$

whence the rôle of ν_2 can be played by any linear combination of $\frac{1}{2\kappa^2} - \ell$ and $\frac{1}{2\kappa^2} \mp \mu$. The third derivative $\frac{3}{4}\kappa^3$ is non-zero; this also follows from $F^{(4)} \equiv 6\kappa^2 \neq 0$.

Note that for all three degenerate Hamiltonian Hopf bifurcations the Hamiltonian (19) does provide a full C^∞-versal unfolding, with modal parameter $\nu_3 = -\lambda_1$. However, putting $\lambda_1 = 0$ results in topological co-dimension 3 instead of 2, see again [19].

3.5. Bifurcation diagram for $\kappa = 0$

We briefly discuss here the case $\kappa = 0$. Note that this case is degenerate: higher order terms in $H_{N,L}$ may change the results obtained here. Moreover, fibres may contain non-compact connected components.

An analysis along the lines of Section 3.3 shows that there are no cusp bifurcations or supercritical Hamiltonian Hopf bifurcations. We find three families of centre-saddle bifurcations $\mathbf{CS}_k^{\kappa=0}$, $k = 1, 2, 3$, whose pairwise common boundaries correspond to three families of subcritical Hamiltonian Hopf bifurcations $(\mathbf{HH}_k^-)^{\kappa=0}$, $k = 1, 2, 3$. Their parametrisations are given in Table 4 and they are depicted in Figs. 5 and 6. Note that the bifurcation diagram for $\kappa = 0$ can be obtained from the one for $\kappa \neq 0$ by considering the limit of each bifurcation family for $\kappa \to 0$ and ignoring the families that exist only for $\lambda > \frac{1}{2\kappa}$.

4. Critical values of the energy–momentum mapping

We now focus on the set of critical values $\mathcal{C}$ of the *energy–momentum mapping*

$$\mathcal{EM} : \mathbb{R}^6 \longrightarrow \mathbb{R}^3$$

defined in (6), i.e. with components N, L and H. Note that the diffeomorphism

$$(\mu, \ell, h) \mapsto (\mu, \frac{\ell + \mu}{2}, h)$$

of $\mathbb{R}^3$ maps $\mathcal{C}$ to the set of critical values of

$$(N, J, H) : \mathbb{R}^6 \longrightarrow \mathbb{R}^3\ ;$$

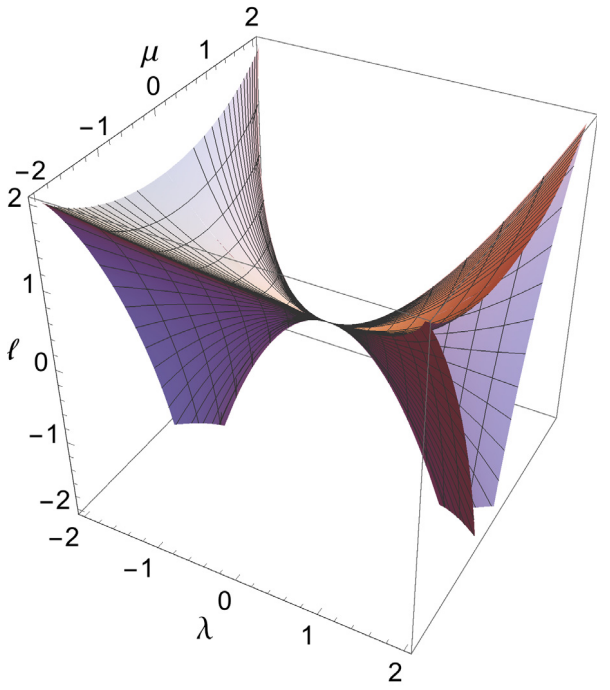

Fig. 5. Bifurcation diagram for $\kappa = 0$ in (λ, μ, ℓ) space. One may think of this as obtained from Fig. 3 by sending the triangle of cusp and degenerate Hamiltonian Hopf bifurcations from $\lambda = \frac{1}{2}$ to $\lambda = \infty$ (and the supercritical Hamiltonian Hopf bifurcations beyond).

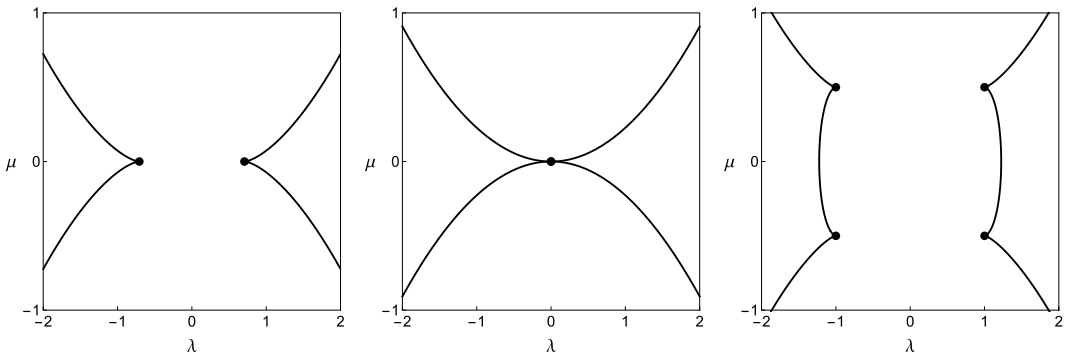

Fig. 6. Bifurcation curves for $\kappa = 0$ and fixed values of ℓ in (λ, μ)-space. From left to right: $\ell = -\frac{1}{2}$, $\ell = 0$ and $\ell = \frac{1}{2}$. The • mark subcritical Hamiltonian Hopf bifurcations (except for the one at $(\lambda, \mu, \ell) = (0, 0, 0)$ corresponding to the central equilibrium in 1:1:−2 resonance).

in fact the whole ramified torus bundle defined by (6) turns into the ramified torus bundle defined by (N, J, H). It is only the way that the toral fibres are orbits of (12) and (14) that is affected by the global isotropy $\mathbb{Z}_2 = \{(0, 0), (\frac{1}{2}, \frac{1}{2})\}$ – the $\mathbb{T}^2$-action (12) runs through regular fibres twice.

The parameter λ depends on the values $N = \mu$ and $L = \ell$ through (20), which defines a diffeomorphism

$$(\delta, \mu, \ell) \quad \mapsto \quad (\lambda, \mu, \ell)$$

of $\mathbb{R}^3$ that relates the bifurcation diagram detailed in Proposition 11 to the bifurcation diagram in terms of (δ, μ, ℓ). While the latter is equal to the former when $\lambda_1 = \lambda_2 = 0$ – the situation we concentrate on in Section 4.2 – it is instructive to compare the intersections $\lambda = \delta$ in Figs. 9 and 10 with Fig. 1 where the detuning δ is fixed, but $(\lambda_1, \lambda_2) \neq (0, 0)$ whence the vertical planes $\lambda = \delta$ get 'tilted' to the planes $\lambda = \delta + \lambda_1\mu + \lambda_2\ell$ with constant δ.

Similarly, we can replace the normal form $H = H^{\delta}_{N,L}$ defined in (19) by the (simplified) reduced Hamiltonian function $\mathcal{H}_\lambda$ of (21) expressed in co-ordinates q_i, p_i, $i = 1, 2, 3$ as the diffeomorphism

$$(\mu, \ell, h) \quad \mapsto \quad \left(\mu, \ell, h - \alpha\ell - \beta\mu - \tfrac{1}{2}\gamma_1\mu^2 - \gamma_2\mu\ell - \tfrac{1}{2}\gamma_3\ell^2\right)$$

Table 4
Bifurcation families for $\kappa = 0$. Here, the quantities $\mu_\pm$ are given by $\mu_\pm^2 = -3a^2 + 6a\lambda^2 - 2\lambda^4 \mp 2|\lambda|(\lambda^2 - 2a)^{3/2}$ and can be obtained from Eq. (50) by setting $\kappa = 0$.

Family	Parametrisation (λ, μ, ℓ)	Parameter ranges
Centre-Saddle		
$\mathbf{CS}_1^{\kappa=0}$	$(\lambda, -\mu_-, 3a - \lambda^2)$	$\lambda \in \mathbb{R}_*$, $0 < a < \lambda^2/2$
$\mathbf{CS}_2^{\kappa=0}$	$(\lambda, \mu_-, 3a - \lambda^2)$	$\lambda \in \mathbb{R}_*$, $0 < a < \lambda^2/2$
$\mathbf{CS}_3^{\kappa=0}$	$(\lambda, \pm\mu_+, 3a - \lambda^2)$	$\lambda \in \mathbb{R}_*$, $4\lambda^2/9 < a < \lambda^2/2$
Hamiltonian Hopf (subcritical)		
$(\mathbf{HH}_1^-)^{\kappa=0}$	$(\lambda, \frac{1}{2}\lambda^2, \frac{1}{2}\lambda^2)$	$\lambda \in \mathbb{R}_*$
$(\mathbf{HH}_2^-)^{\kappa=0}$	$(\lambda, -\frac{1}{2}\lambda^2, \frac{1}{2}\lambda^2)$	$\lambda \in \mathbb{R}_*$
$(\mathbf{HH}_3^-)^{\kappa=0}$	$(\lambda, 0, -\lambda^2)$	$\lambda \in \mathbb{R}_*$

of $\mathbb{R}^3$ maps critical values to critical values. In the sequel we therefore work with the energy–momentum mapping

$$\mathcal{EM} \;=\; (N, L, \mathcal{H}_\lambda)\ , \tag{45}$$

the values of which we keep denoting by $(\mu, \ell, h) \in \mathbb{R}^3$. We consider only the case $\kappa \neq 0$ and the scaling (22) allows us to restrict to

$$\kappa \;=\; 1\ , \tag{46}$$

the value which was also used for Table 3 and Figs. 3 and 4.

4.1. Amended bifurcation diagram

The critical values of (45) correspond to values (μ, ℓ, h) of the internal parameters and energy for which the level set $\mathcal{H}_\lambda^{-1}(h)$ of the reduced Hamiltonian either has a tangency with the reduced space $P_{\mu\ell}$ or goes through the singular point of $\mathcal{P}_{\mu\ell}$. Recall from Proposition 5 that the reduced phase space $\mathcal{P}_{\mu\ell}$ is singular at $(R_{\min}, 0, 0)$ for $\ell = |\mu|$ or $\mu = 0$, $\ell \leq 0$, where $R_{\min} = \max(|\mu|, \ell)$. From (21) with $\kappa = 1$ we find that the value h_c of the energy for which $\mathcal{H}_\lambda^{-1}(h)$ goes through the singular point is

$$h_c \;=\; \lambda R_{\min} \,+\, \tfrac{1}{2}R_{\min}^2 \;=\; \begin{cases} \lambda\ell + \frac{1}{2}\ell^2 & \text{for } \mu = \pm\ell,\ \ell \geq 0 \\ 0 & \text{for } \mu = 0,\ \ell \leq 0. \end{cases}$$

This gives three curves of critical values of $\mathcal{EM}$, each one parametrised by ℓ. Mirroring the notation for the normal modes in Table 1 we denote by $\mathcal{C}_{23}$ the curve corresponding to $\mu = \ell$, $\ell > 0$, parametrising the normal 1-mode, by $\mathcal{C}_{13}$ the curve corresponding to $\mu = -\ell$, $\ell > 0$, parametrising the normal 2-mode and by $\mathcal{C}_{12}$ the curve corresponding to $\mu = 0$, $\ell < 0$, parametrising the normal 3-mode, noting that $\mathcal{EM}(C_{ij}) = \mathcal{C}_{ij}$ for $ij = 12, 13, 23$. Depending on the topology of $\mathcal{H}_\lambda^{-1}(h_c) \cap \mathcal{P}_{\mu\ell}$ (parts of) these curves could be attached to a surface of critical values or be transversally isolated, in the sense that a neighbourhood of a point of such a curve contains only critical values from the same curve. We denote by $\mathcal{C}_{ij}^0$ the subset of the curve $\mathcal{C}_{ij}$ where it is transversally isolated and we refer to such subset as *thread*. Moreover, we denote by $\mathcal{C}_{ij}^+ \subseteq \mathcal{C}_{ij}$ the subset where $h_c > h_{\min}$; here $h_{\min}$ is the minimal value of $\mathcal{H}_\lambda$ for given (μ, ℓ). The minimum $h_{\min}$ of $\mathcal{H}_\lambda$ on $\mathcal{P}_{\mu\ell}$ depends continuously on μ and ℓ whence necessarily $\mathcal{C}_{ij}^0 \subseteq \mathcal{C}_{ij}^+$.

The topology of $\mathcal{H}_\lambda^{-1}(h_c) \cap \mathcal{P}_{\mu\ell}$, and subsequently of the fibre $\mathcal{EM}^{-1}(\mu, \ell, h_c)$ depends on the slope of $\mathcal{H}_\lambda^{-1}(h_c)$ relative to the slope of $\mathcal{P}_{\mu\ell}$ at the singular point. Recall from the discussion in Section 3.2 that for each value of (μ, ℓ) such that the reduced space $\mathcal{P}_{\mu\ell}$ has a singular point, there is an interval of values of λ such that the connected component of $\mathcal{H}_\lambda^{-1}(h_c) \cap \mathcal{P}_{\mu\ell}$ that goes through the singular point is a topological (non-smooth) circle consisting of the dynamically unstable singular point and its stable=unstable manifold. We note here that such critical values (μ, ℓ, h_c) that have $\mathcal{H}_\lambda^{-1}(h_c) \cap \{Y = 0\}$ in the 'interior' of $\mathcal{P}_{\mu\ell}$, compare with Fig. 2(middle), lie on the thread $\mathcal{C}_{ij}^0$ for the corresponding $ij \in \{12, 13, 23\}$ and thus in the interior of the image of $\mathcal{EM}$.

Reconstructing the $\mathbb{T}^2$-action Φ over a topological (non-smooth) circle $\mathcal{H}_\lambda^{-1}(h_c) \cap \mathcal{P}_{\mu\ell}$ gives that the resulting singular fibre is the Cartesian product of a two-dimensional pinched torus, see Fig. 7, with a (smooth) torus $\mathbb{T}^1$. The latter is the normal mode that had been reduced to the singular equilibrium on $\mathcal{P}_{\mu\ell}$ and the former constitutes its stable=unstable manifold. Specifically, the condition for $\mathcal{H}_\lambda^{-1}(h_c) \cap \mathcal{P}_{\mu\ell}$ to be a topological circle is $|X_1'(R_{\min})| < |X_2'(R_{\min})|$. Since

$$F''(R_{\min}) \;=\; 2\left(X_1'(R_{\min})^2 - X_2'(R_{\min})^2\right)$$

we get the equivalent condition $F''(R_{\min}) < 0$. For fixed values (μ, ℓ) such that $\mathcal{P}_{\mu\ell}$ is singular we consider the values of λ such that $\mathcal{H}_\lambda^{-1}(h_c) \cap \mathcal{P}_{\mu\ell}$ is a topological circle. Evaluating for $h = h_c$ that

$$F''(R_{\min}) \;=\; 2\lambda^2 \,+\, 4\lambda R_{\min} \,+\, 2(\ell + R_{\min}^2 - 3R_{\min})\ ,$$

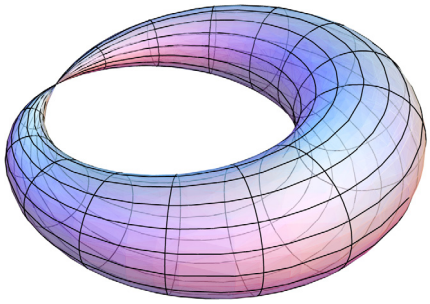

Fig. 7. Two-dimensional pinched torus.

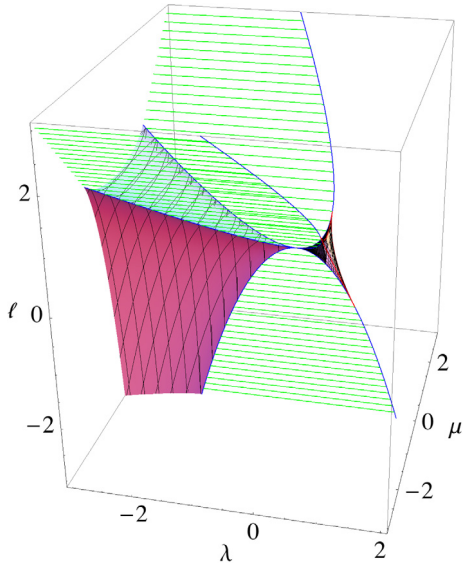

Fig. 8. Amended bifurcation diagram. The horizontal lines represent intervals of values of λ for which the fibre of $\mathcal{H}_\lambda$ going through the singular point of $\mathcal{P}_{\mu\ell}$ is a topological circle, i.e. the singular point is an unstable equilibrium.

we conclude that there is exactly one λ-interval where $F''(R_{\min}) < 0$, lying between the two real roots of $F''(R_{\min})$. The endpoints of the λ-interval correspond to Hamiltonian Hopf bifurcations and Lemma 10 allows us to distinguish the supercritical from the subcritical ones. In case $\mu = 0$, $\ell < 0$, the interval is $-\sqrt{-\ell} \le \lambda \le \sqrt{-\ell}$. For $-1 < \ell < 0$ both ends of the interval correspond to subcritical Hamiltonian Hopf bifurcations. For $\ell < -1$ the right end $\lambda = \sqrt{-\ell}$ corresponds to a supercritical Hamiltonian Hopf bifurcation while the left end $\lambda = -\sqrt{-\ell}$ corresponds to a subcritical Hamiltonian Hopf bifurcation. In case $\ell = |\mu| > 0$, the interval is $-\sqrt{2\ell} - \ell \le \lambda \le \sqrt{2\ell} - \ell$. For $0 < \ell < 1$ both ends of this interval correspond to subcritical Hamiltonian Hopf bifurcations. For $\ell > 1$ the right end $\lambda = \sqrt{2\ell} - \ell$ corresponds to a supercritical Hamiltonian Hopf bifurcation while the left end $\lambda = -\sqrt{2\ell} - \ell$ corresponds to a subcritical Hamiltonian Hopf bifurcation. These λ-intervals are represented by the horizontal lines in Fig. 8 for equally spaced values of ℓ. It is for these values that pinched tori occur — not a bifurcation, but a critical element for the description of the dynamics.

We call the diagram in Fig. 8 the *amended bifurcation diagram*. It combines the bifurcation diagram, discussed in Section 3.3, and the values (λ, μ, ℓ) for which $\mathcal{H}_\lambda^{-1}(h_c) \cap \mathcal{P}_{\mu\ell}$ is a topological (non-smooth) circle. Each point in this diagram thus corresponds to a critical value of the energy–momentum mapping (45) and the diagram is used as a starting point for deducing the structure of the set of critical values of $\mathcal{EM}$.

4.2. Set of critical values of $\mathcal{EM}$

To obtain the set of critical values $\mathcal{C}$ of the energy–momentum mapping $\mathcal{EM}$ we consider different cases for the parameters δ, λ_1, λ_2 appearing in the Hamiltonian function. For fixed values of δ, λ_1, λ_2 the relation $\lambda = \delta + \lambda_1\mu + \lambda_2\ell$ in (20) defines an embedding of the (μ, ℓ)-plane into the (λ, μ, ℓ)-space. The intersection of this embedded plane with the amended bifurcation diagram provides information that allows us to reconstruct a large part of $\mathcal{C}$. In this section, we determine $\mathcal{C}$ for different choices of δ while fixing $\lambda_1 = \lambda_2 = 0$, that is, we consider only vertical planes $\lambda =$ constant in

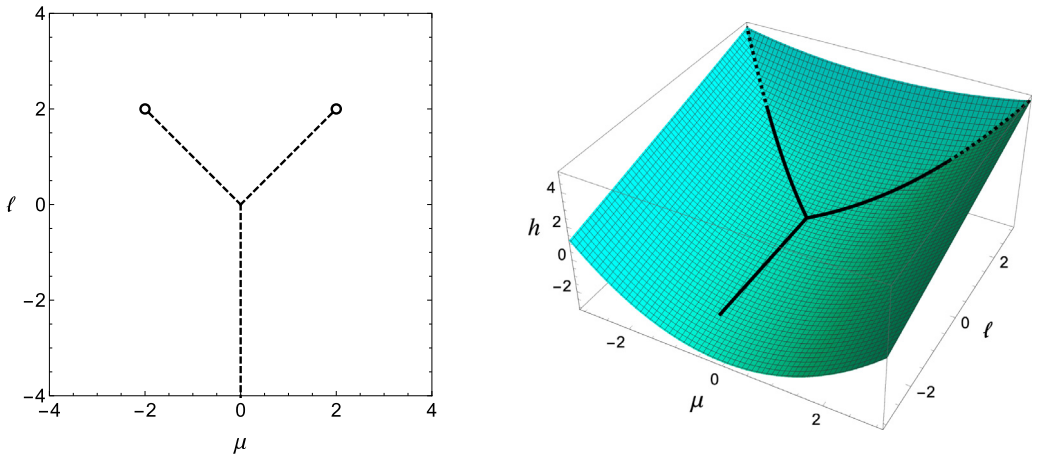

Fig. 9. Left: intersection of the plane $\lambda = 0$ with the amended bifurcation diagram. The dashed lines parametrise families of unstable periodic orbits, the $\circ$ stand for supercritical Hamiltonian Hopf bifurcations. Right: set $\mathcal{C}$ of critical values of $\mathcal{EM}$ for $\delta = \lambda_1 = \lambda_2 = 0$. The three solid lines lie above the surface and at the two dashed curves the otherwise smooth surface $\mathcal{B}$ has two creases; the transition is at the two supercritical Hamiltonian Hopf bifurcations. Values in the interior of each solid curve correspond to the Cartesian product of a two-dimensional pinched torus with $\mathbb{T}^1$; values on the dashed lines to $\mathbb{T}^1$; values on the surface to $\mathbb{T}^2$; regular values above the surface to $\mathbb{T}^3$.

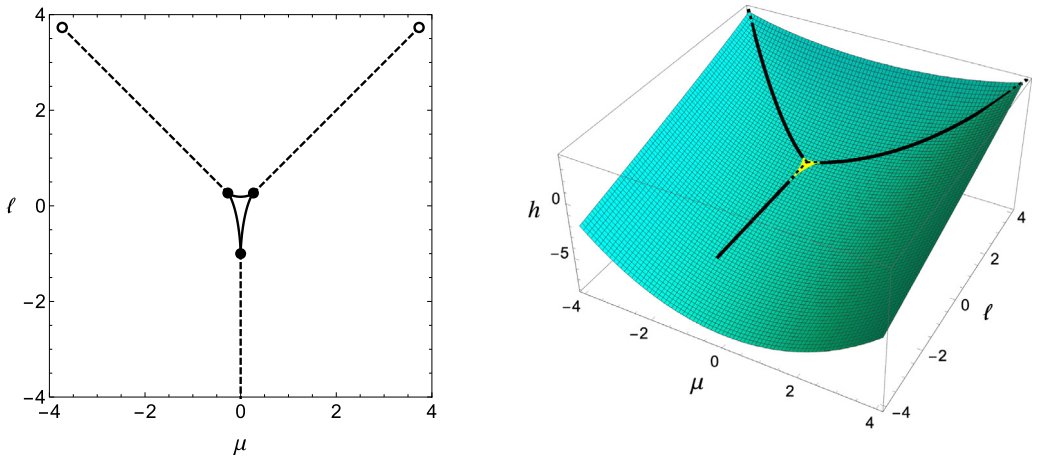

Fig. 10. Left: intersection of the plane $\lambda = -1$ with the amended bifurcation diagram. The solid lines parametrise families of centre-saddle bifurcations, the $\bullet$ stand for subcritical Hamiltonian Hopf bifurcations, and the $\circ$ stand for supercritical Hamiltonian Hopf bifurcations. Right: set of critical values $\mathcal{C}$ for $\delta = -1$, $\lambda_1 = \lambda_2 = 0$. For an enlargement of the central region see Fig. 11.

the (λ, μ, ℓ)-space. The study of such vertical planes gives a complete description of possible behaviours also for slightly tilted planes; the only exception is the (degenerate) $\lambda = 1/(2\kappa)$ where a slight tilt qualitatively changes $\mathcal{C}$. For more strongly tilted planes, arguments similar to the ones we use below allow to determine $\mathcal{C}$ for any other choice of δ, λ_1, λ_2 and also for the case $\kappa = 0$. Nevertheless, a complete description of all possible cases is beyond the aim of this paper.

4.2.1. Case $\boldsymbol{\delta = \lambda_1 = \lambda_2 = 0}$

In this 'undetuned' case the (μ, ℓ)-plane embeds as the $(\lambda{=}0)$-plane in the (λ, μ, ℓ)-space. We can deduce a large part of $\mathcal{C}$ by checking the intersection of the $(\lambda{=}0)$-plane with the amended bifurcation diagram in Fig. 8. The plane $\lambda = 0$ intersects the three surfaces of h-isolated critical values along the lines $\mu = \pm\ell$, $0 \le \ell \le 2$ and $\mu = 0, \ell \le 0$, see Fig. 9(left). At $\ell = 2$ the two lines $\mu = \pm\ell$ end at supercritical Hamiltonian Hopf bifurcations while the line $\mu = 0$ extends indefinitely. These three lines give three curves of critical values of $\mathcal{EM}$, where the value of h_c has to also be taken into account as discussed in Section 4.1. In particular, the curves $\mathcal{C}_{23}$ and $\mathcal{C}_{13}$ have parts $\mathcal{C}^0_{23} = \mathcal{C}^+_{23}$ and $\mathcal{C}^0_{13} = \mathcal{C}^+_{13}$ that end at supercritical Hamiltonian Hopf bifurcations while $\mathcal{C}_{12} = \mathcal{C}^0_{12}$ extends indefinitely.

The parts $\mathcal{C}_{ij} \backslash \mathcal{C}^+_{ij}$, $ij = 23, 13$ have $h_c = h_{\min}$ – here the normal 1-mode respectively the normal 2-mode is stable as $\mathcal{H}_0^{-1}(h_{\min}) \cap \mathcal{P}_{\mu\ell}$ is a single point, the singular point reduced from the normal mode. The rest of $\mathcal{C}$ consists of values where the energy level touches the reduced space from outside, in a regular point of $\mathcal{P}_{\mu\ell}$. This implies that for such a value the

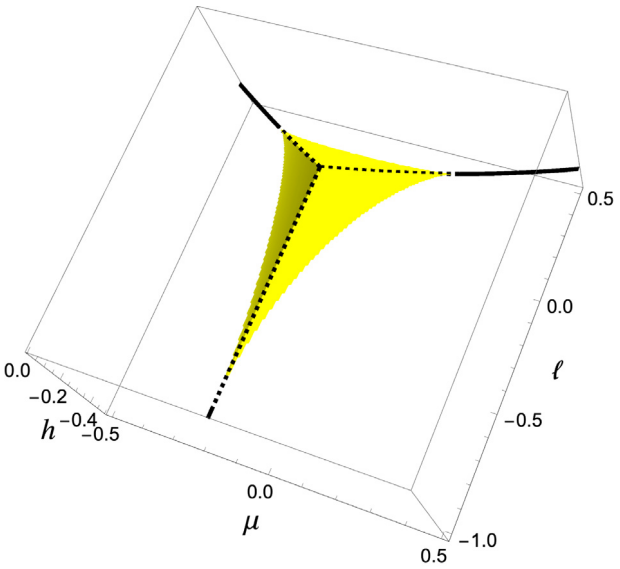

Fig. 11. Detail of $\mathcal{C}$ for $\lambda = -1$.

energy $\mathcal{H}_0$ is at minimum for given (μ, ℓ) and the set of such values $(\mu, \ell, h_{\min})$ yields the boundary of the image of $\mathcal{EM}$. We denote by $\mathcal{B} \subseteq \mathcal{C}$ the surface $\{(\mu, \ell, h_{\min}) : (\mu, \ell) \in \mathbb{R}^2\}$, note that $\mathcal{B}$ also contains the lines $\mathcal{C}_{ij} \backslash \mathcal{C}_{ij}^+$, $ij = 23, 13$. The set $\mathcal{C}$ of critical values is shown in Fig. 9(right).

The set $\mathcal{R}$ of regular values (μ, ℓ, h) of $\mathcal{EM}$ parametrises the Lagrangian $\mathbb{T}^3$ in phase space. Critical values on $\mathcal{B}$ parametrise smooth $\mathbb{T}^2$ in phase space which are also Φ-orbits, provided that they do not belong to $\mathcal{C}_{13}$ or $\mathcal{C}_{23}$. Critical values on $\mathcal{C}_{13} \cap \mathcal{B}$ or $\mathcal{C}_{23} \cap \mathcal{B}$ lift to $\mathbb{T}^1$. Critical values along the three threads of critical values $\mathcal{C}_{ij}^0$ correspond to singular fibres, the Cartesian product of a two-dimensional pinched torus, see Fig. 7, with a $\mathbb{T}^1$, the latter associated to a circle action that acts freely on the fibre. Note that there is no globally defined circle action arising from a linear combination of X_N and X_L that acts freely on fibres over all three curves of critical values. Finally, the critical value $(\mu, \ell, h) = (0, 0, 0)$, where the three threads meet, corresponds to a singular fibre, which can be described as a $\mathbb{T}^3$ where a $\mathbb{T}^2$ orbit has been 'pinched' to a point.

Remark 12. It is the undetuned case where the central equilibrium is in 1:1:−2 resonance and the level set $\mathcal{H}_0^{-1}(0)$ passes through the cuspidal singularity of $\mathcal{P}_{00}$, yielding a topological (non-smooth) circle. Hence, in three degrees of freedom each regular point gets a $\mathbb{T}^2$ attached and all these form the stable=unstable manifold of the central equilibrium, which has isotropy $\mathbb{T}^2$ under (11), revealing the 1:1:−2 resonant equilibrium to be unstable (despite being linearly stable). This is reminiscent of both the 'phantom kiss' at a periodic orbit undergoing a 1:3 normal-internal resonance, compare with [1,14], and the normal 1:−2 resonance in two degrees of freedom, compare with [3,9].

4.2.2. Case $\boldsymbol{\delta < 0}$, $\boldsymbol{\lambda_1 = \lambda_2 = 0}$

Adding a small detuning $\delta \neq 0$ qualitatively modifies the set of critical values only in a neighbourhood of the origin. We first consider the case $\delta < 0$, $\lambda_1 = \lambda_2 = 0$. Here the (μ, ℓ)-plane embeds in (λ, μ, ℓ)-space as the plane $\lambda = \delta < 0$, and all such planes have qualitatively the same intersection with the amended bifurcation diagram.

A plane $\lambda = \delta$ intersects the amended bifurcation diagram along three straight lines and a curvilinear triangle $\mathcal{D}$, see Fig. 10(left). Each of the straight lines joins $\mathcal{D}$ at a vertex corresponding to a subcritical Hamiltonian Hopf bifurcation. The two straight lines parametrised by $\mu = \pm\ell$ with $1 - \lambda - \sqrt{1 - 2\lambda} < \ell < 1 - \lambda + \sqrt{1 - 2\lambda}$ end at supercritical Hamiltonian Hopf bifurcations. The straight line parametrised by $\ell < -\lambda^2$ at $\mu = 0$ extends indefinitely. The edges of $\mathcal{D}$ are the intersections with the surfaces of centre-saddle bifurcations.

The set of critical values $\mathcal{C}$ is depicted in Fig. 10(right). Away from the origin, the description of $\mathcal{C}$ from Section 4.2.1 can be repeated verbatim for this case. However, the situation is different near the origin, see Fig. 11. In the set of critical values we note the appearance of a tetrahedral surface $\mathcal{T}$ of critical values, corresponding to the appearance of $\mathcal{D}$ in the intersection of the plane $\lambda = \delta$ with the amended bifurcation diagram. The surface $\mathcal{T}$ separates the set $\mathcal{R}$ of regular values into two connected components: $\mathcal{R}'$ outside $\mathcal{T}$ and $\mathcal{R}''$ inside $\mathcal{T}$. Values in $\mathcal{R}'$ lift to $\mathbb{T}^3$. However, values $v = (\mu, \ell, h) \in \mathcal{R}''$ correspond to the union of two disjoint $\mathbb{T}^3$ in phase space. We denote by $\mathbb{T}^3_A(v)$ and $\mathbb{T}^3_B(v)$ the two resulting disjoint families of tori parametrised by $v \in \mathcal{R}''$.

The curvilinear triangle $\mathcal{D}$ of centre-saddle bifurcations embeds in $\mathcal{T}$ as the union of three curved edges $\mathcal{D}'$ that splits the "upper" and "lower" parts of $\mathcal{T}$. The "upper" part of $\mathcal{T}$ is visible in Fig. 11. It consists of three faces that we denote by

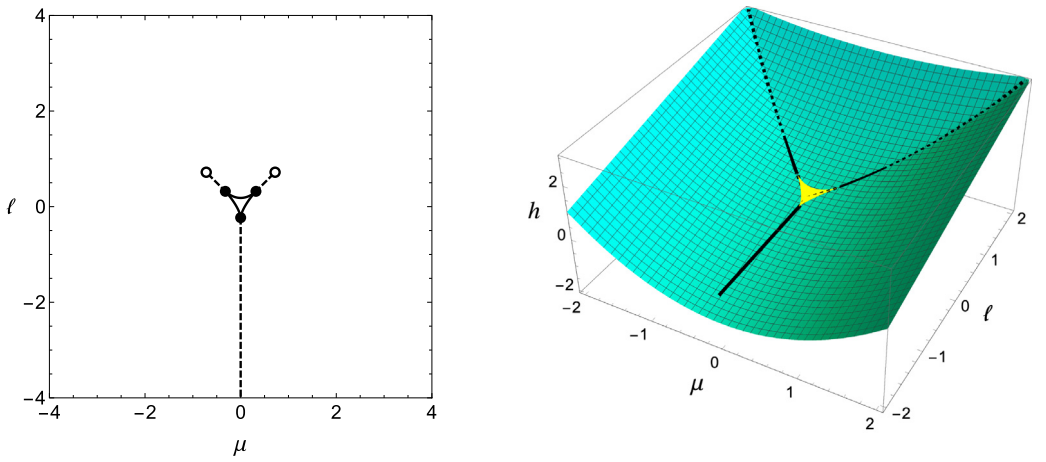

Fig. 12. Intersection of the plane $\lambda = 0.48$ with the amended bifurcation diagram and the corresponding set of critical values $\mathcal{C}$.

$\mathcal{F}_+$, $\mathcal{F}_-$ and $\mathcal{F}_0$, respectively, and the three straight lines $\mathcal{C}^+_{ij}\backslash\mathcal{C}^0_{ij}$ of stable normal modes. To be precise, $\mathcal{F}_0$ has $\ell > |\mu|$ and lies between $\mathcal{C}_{13}$, $\mathcal{C}_{23}$ and $\mathcal{D}'$ while $\mathcal{F}_+$ has $\mu > \max(\ell, 0)$ and lies between $\mathcal{C}_{12}$, $\mathcal{C}_{23}$ and $\mathcal{D}'$ and $\mathcal{F}_-$ has $\mu < \min(-\ell, 0)$ and lies between $\mathcal{C}_{12}$, $\mathcal{C}_{13}$ and $\mathcal{D}'$. We denote by $\mathcal{F}^\circ_e$ the union of the faces $\mathcal{F}_{0,\pm}$ and by $\mathcal{F}_e$ the union of $\mathcal{F}^\circ_e$ with the pairwise common topological boundaries of $\mathcal{F}_{0,\pm}$ (the dashed lines in Fig. 11), so $\mathcal{F}_e$ constitutes the "upper" part of $\mathcal{T}$. The "lower" part consists of a single face $\mathcal{F}_h$ with topological boundary $\mathcal{D}'$. Note that in all four cases we do not consider the topological boundary of a face to belong to the face.

Values on the "upper" part $\mathcal{F}^\circ_e$ lift to the disjoint union of a $\mathbb{T}^2$ and a $\mathbb{T}^3$. Here, one of the families $\mathbb{T}^3_{A,B}(v)$ in $v \in \mathcal{R}''$ shrinks down to a $\mathbb{T}^2$ as v approaches $\mathcal{F}^\circ_e$. This allows us to 'globally' distinguish the two families: we take $\mathbb{T}^3_B(v)$ to be the family that shrinks down to $\mathbb{T}^2$ and $\mathbb{T}^3_A(v)$ the family that can be smoothly continued outside of $\mathcal{R}''$ to the regular $\mathbb{T}^3$-fibration over $\mathcal{R}'$. Dynamically, the lower dimensional invariant torus $\mathbb{T}^2$ is elliptic. The pairwise common boundaries of $\mathcal{F}_{0,\pm}$ meet at the origin. The origin lifts to the disjoint union of a point, the central equilibrium, and a $\mathbb{T}^3$ in phase space. Other values on these pairwise common boundaries lift to the disjoint union of a normal mode (a $\mathbb{T}^1$) and a $\mathbb{T}^3$.

Values on the "lower" part $\mathcal{F}_h$ lift to a connected singular fibre. The singular fibre is the Cartesian product of a figure eight with a $\mathbb{T}^2$, that is, it corresponds to the two disjoint families $\mathbb{T}^3_A(v)$ and $\mathbb{T}^3_B(v)$ in $\mathcal{R}''$ getting glued together along a common $\mathbb{T}^2$. Dynamically, this lower dimensional invariant torus $\mathbb{T}^2$ is hyperbolic and the two glued $\mathbb{T}^3$ correspond to its stable=unstable manifold. The face $\mathcal{F}_h$ meets each one of the faces $\mathcal{F}_{0,\pm}$ along a family of centre-saddle bifurcations (an edge of $\mathcal{D}'$), where the hyperbolic $\mathbb{T}^2$ from $\mathcal{F}_h$ and the elliptic $\mathbb{T}^2$ from $\mathcal{F}^\circ_e$ meet and disappear. Moving on $\mathcal{F}_h$ towards an edge of $\mathcal{D}'$, the component $\mathbb{T}^3_B$ (glued with $\mathbb{T}^3_A$ to form the corresponding singular fibre) shrinks and then disappears at the edge of $\mathcal{D}'$.

Remark 13. It is instructive to have a look at the quantitative changes that occur as δ increases towards 0 before the qualitative change at the case $\delta = 0$ discussed before. Indeed for $\delta \nearrow 0$ the tetrahedral surface $\mathcal{T}$ gets smaller and smaller, shrinking to the critical value $(\mu, \ell, h) = (0, 0, 0)$ where the three threads that we have seen to exist for $\delta = 0$ meet. For $\delta > 0$ another tetrahedral set $\mathcal{T}'$ emerges, 'flipped upside-down' compared to $\mathcal{T}$. Thus, while passing through the 1:1:−2 resonance, the three straight lines $\mathcal{C}^+_{ij}\backslash\mathcal{C}^0_{ij}$ parametrising the stable normal modes of the elliptic central equilibrium shrink down (and re-grow) as the central equilibrium momentarily loses its stability at the 1:1:−2 resonance itself.

4.2.3. *Cases* $\boldsymbol{\delta > 0}$, $\boldsymbol{\lambda_1 = \lambda_2 = 0}$

We now turn our attention to the case $\delta > 0$. Here the (μ, ℓ)-plane embeds in (λ, μ, ℓ)-space as the plane $\lambda = \delta > 0$ and we must consider three subcases depending on the value of δ. Indeed, when comparing with the case $\delta < 0$ we see that the planes $\lambda = \delta > 0$ intersect the amended bifurcation diagram in five different ways. We omit the transitional cases $\delta = \frac{1}{2}$, $\delta = 1$ and concentrate on the three open intervals $]0, \frac{1}{2}[$, $]\frac{1}{2}, 1[$ and $]1, \infty[$ of small, intermediate and large positive detuning δ.

Case $\boldsymbol{0 < \delta < \frac{1}{2}}$. The intersection of the plane $\lambda = \delta$ with the amended bifurcation diagram as depicted in Fig. 12(left) is qualitatively the same as in the case $\delta < 0$. The set of critical values $\mathcal{C}$ as depicted in Fig. 12(right) is also similar, with the only difference that the tetrahedral set $\mathcal{T}'$ of critical values has been flipped upside-down, see Remark 13. Therefore, it is now the "upper" part where we find the face $\mathcal{F}_h$ with hyperbolic $\mathbb{T}^2$, while the "lower" part $\mathcal{F}_e$ consists of three creases parametrising the normal modes joined by three faces $\mathcal{F}_{0,\pm}$ where we find elliptic $\mathbb{T}^2$. The discussion in Section 4.2.2 carries over *mutatis mutandi*.

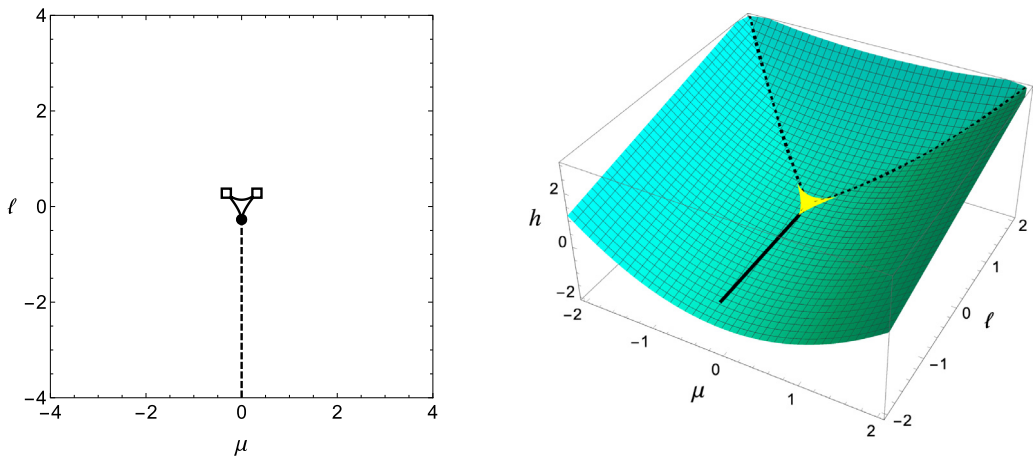

Fig. 13. Left: intersection of the plane $\lambda = 0.52$ with the amended bifurcation diagram. The □ stand for cusp bifurcations and the • marks the subcritical Hamiltonian Hopf bifurcation. Right: corresponding set of critical values $\mathcal{C}$ of $\mathcal{EM}$. For an enlargement of the central region see Fig. 14.

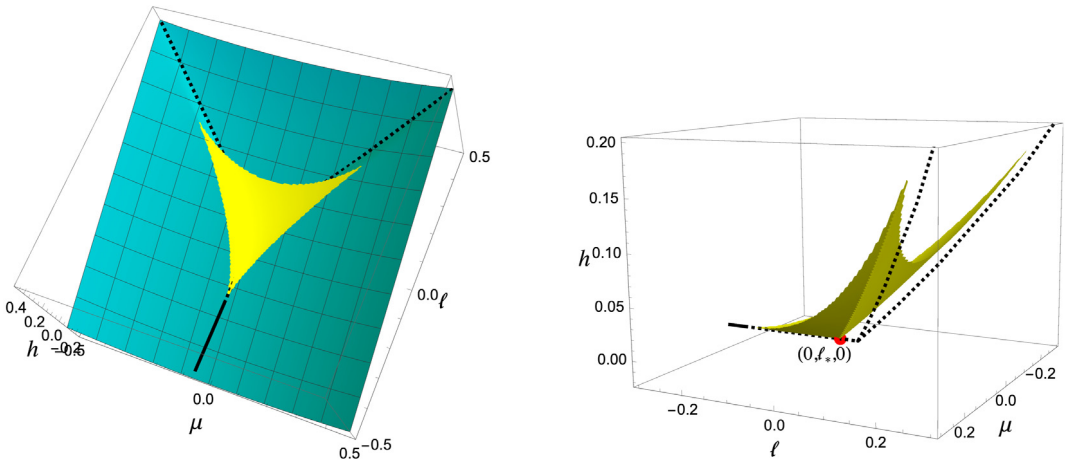

Fig. 14. Two views of $\mathcal{C}$ for $\lambda = 0.52$ focusing on $\mathcal{T}''$. At the right panel we are not showing the whole set $\mathcal{B}$ so as to make more prominent the features of $\mathcal{T}''$ – we are drawing however the curves $\mathcal{C}_{12}$, $\mathcal{C}_{23}$, $\mathcal{C}_{13}$ and we note that $\mathcal{C}_{13}$, $\mathcal{C}_{23}$, and the part of $\mathcal{C}_{12}$ between the origin and $(0, \ell_*, 0)$ are contained in $\mathcal{B}$. Note that $\mathcal{T}''$ touches $\mathcal{B}$ only along the 'creases' $\mathcal{L}_+$ and $\mathcal{L}_-$ of $\mathcal{T}''$ that start at $(0, \ell_*, 0)$ and end at the two topmost 'horns'.

Remark 14. It is instructive to have a look at the quantitative changes that occur as δ increases towards $\frac{1}{2}$. Indeed, exactly at $\delta = \frac{1}{2}$ the two vertices of the tetrahedral surface $\mathcal{T}'$ correspond to degenerate Hamiltonian Hopf bifurcations. Moreover, between these two vertices extends a whole curve of cusp bifurcations $\mathbf{CB}_3$. This is probably the most important difference to considering 'tilted' planes with $(\lambda_1, \lambda_2) \neq (0, 0)$ which e.g. for small $\lambda_2 > 0$ (and $\lambda_1 = 0$) 'first' contain two degenerate Hamiltonian Hopf bifurcations (for an exceptional value $\delta^* < \frac{1}{2}$) and (increasing δ slightly above δ^*) contain four isolated values of cusp bifurcations. For $\lambda_1 \neq 0$ the two degenerate Hamiltonian Hopf bifurcations lie in different tilted planes.

For $\delta \nearrow \frac{1}{2}$ (with $\lambda_1 = \lambda_2 = 0$) the face $\mathcal{F}_0$ of $\mathcal{T}'$ moves closer and closer to the surface $\mathcal{B}$ of minimal energy values, until at $\delta = \frac{1}{2}$ the intersection $\mathcal{T}' \cap \mathcal{B}$ consists of $\mathcal{F}_0$, of the values $(\mu, \ell, h) = (\frac{1}{2}, \pm\frac{1}{2}, \frac{1}{2})$ of degenerate Hamiltonian Hopf bifurcations and $(\mu, \ell, h) = (0, 0, 0)$ of the central equilibrium, and of the parts of $\mathcal{C}_{13}, \mathcal{C}_{23}$ that extend between the central equilibrium and one of the degenerate Hamiltonian Hopf bifurcations. For $\delta > \frac{1}{2}$ we denote the tetrahedral surface, which no longer contains the origin $(\mu, \ell, h) = (0, 0, 0)$, by $\mathcal{T}''$ and leave the description of its position with respect to $\mathcal{B}$ to case $\frac{1}{2} < \delta < 1$ below.

Case $\frac{1}{2} < \boldsymbol{\delta} < \mathbf{1}$. In the intersection of the plane $\lambda = \delta$ with the amended bifurcation diagram, depicted in Fig. 13(left), the two line segments along $\mu = \pm\ell$ parametrising unstable normal modes have disappeared. Their endpoints, which are supercritical and subcritical Hamiltonian Hopf bifurcations, met at $\delta = \frac{1}{2}$ and for $\delta > \frac{1}{2}$ the corresponding vertices of the curvilinear triangle $\mathcal{D}$ stand for cusp bifurcations.

The changes in the set of critical values, depicted in Fig. 13(right), reflect the changes in the intersection with the amended bifurcation diagram. We focus on the modified part of the set of critical values depicted in Fig. 14. In this

case we 'again' have a tetrahedral surface $\mathcal{T}''$, but its properties are different from the cases described before. The same structure also appears in a detuned 1:1:2 resonance and has been described in [22]. Following the previously introduced terminology, we denote by $\mathcal{R}'$ and $\mathcal{R}''$ the two connected components of $\mathcal{R}$, outside and inside of $\mathcal{T}''$, respectively. Values in $\mathcal{R}'$ lift to $\mathbb{T}^3$. Values in $\mathcal{R}''$ lift to the disjoint union of two $\mathbb{T}^3$ and therefore we can again consider two disjoint families $\mathbb{T}^3_A(v)$ and $\mathbb{T}^3_B(v)$ for $v \in \mathcal{R}''$.

We denote by $\mathcal{F}_h$ the "upper" part of $\mathcal{T}''$ with topological boundary the embedding $\mathcal{D}'$ of $\mathcal{D}$ to $\mathcal{T}''$. Values in $\mathcal{F}_h$ lift to singular fibres where the families $\mathbb{T}^3_A(v)$ and $\mathbb{T}^3_B(v)$ intersect along a hyperbolic lower dimensional invariant torus $\mathbb{T}^2$. Two of the vertices of $\mathcal{D}'$ correspond to cusp bifurcations, and they are part of the intersection $\mathcal{T}'' \cap \mathcal{B}$, while the remaining vertex (with $\mu = 0$, not on $\mathcal{B}$) corresponds to a subcritical Hamiltonian Hopf bifurcation where the thread $\mathcal{C}^0_{12}$ parametrising pinched tori turns into the crease $\mathcal{C}^+_{12}\backslash\mathcal{C}^0_{12}$ of the "lower" part $\mathcal{F}_e$ of the tetrahedron, parametrising the now stable normal 3-mode.

The "lower" part $\mathcal{F}_e$ of $\mathcal{T}''$ has again three faces. Using the same conventions as in Section 4.2.2, we denote these faces by $\mathcal{F}_{0,\pm}$ and we denote by $\mathcal{F}^\circ_e$ their union, noting that $\mathcal{F}^\circ_e \cap \mathcal{B} = \emptyset$. Values on $\mathcal{F}^\circ_e$ lift to the disjoint union of a $\mathbb{T}^2$ and a $\mathbb{T}^3$. The difference with previous cases is that it is not the same $\mathbb{T}^3$-family in $\mathcal{R}''$ that shrinks down to $\mathbb{T}^2$ at each of these faces whence we no longer can make a 'global' choice. Specifically, let $\mathbb{T}^3_A(v)$ be the family that shrinks down to $\mathbb{T}^2$ at the face $\mathcal{F}_+$. Then, the same family $\mathbb{T}^3_A(v)$ shrinks down to $\mathbb{T}^2$ at $\mathcal{F}_-$. However, it is the family $\mathbb{T}^3_B(v)$ that shrinks down to $\mathbb{T}^2$ at $\mathcal{F}_0$. Values on the common topological boundary of $\mathcal{F}_-$ and $\mathcal{F}_+$ (a subset of $\mathcal{C}_{12}$) lift to the disjoint union of the stable normal 3-mode (a smooth $\mathbb{T}^1$) and a $\mathbb{T}^3$.

Thus, after emanating from the central equilibrium, the normal 3-mode parametrised by $\mathcal{C}_{12}\backslash\mathcal{C}^+_{12}$ first is stable with minimal energy $h_{\min} = 0$ until the value

$$(\mu, \ell, h) \;=\; (0, \ell^*, 0) \;\in\; \mathcal{C}_{12} \cap \mathcal{T}'' \cap \mathcal{B}\ , \quad \ell^* \in]-\lambda^2, 0[\ ,$$

then is parametrised by $\mathcal{C}^+_{12}\backslash\mathcal{C}^0_{12} \subseteq \mathcal{T}''$ and loses its stability in the subcritical Hamiltonian Hopf bifurcation at $\mathcal{T}'' \cap \partial\mathcal{C}^0_{12}$. The intersection $\mathcal{T}'' \cap \mathcal{B}$ is formed by $(0, \ell^*, 0)$ and the two values of cusp bifurcations together with the curve segments $\mathcal{L}_+$ and $\mathcal{L}_-$ where $\mathcal{F}_+$ and $\mathcal{F}_-$, respectively, meet with $\mathcal{F}_0$. Values on $\mathcal{L}_\pm$ lift to the disjoint union $\mathbb{T}^2_A(v)\dot\cup\mathbb{T}^2_B(v)$ of two $\mathbb{T}^2$, one being the limit of the family $\mathbb{T}^3_B(v)$ at $\mathcal{F}_0$ and one being the limit of the family $\mathbb{T}^3_A(v)$ at $\mathcal{F}_\pm$. Note that the family $\mathbb{T}^3_A(v)$ can be smoothly continued through the face $\mathcal{F}_0$ (where $\mathbb{T}^3_B(v)$ shrinks down) to the regular $\mathbb{T}^3$-fibration over $\mathcal{R}'$, while the family $\mathbb{T}^3_B(v)$ can be smoothly continued through $\mathcal{F}_+$ or $\mathcal{F}_-$ (where $\mathbb{T}^3_A(v)$ shrinks down).

In the complement of the normal modes parametrised by $\mathcal{C}_{ij}$ the surface $\mathcal{B}$ parametrises invariant 2-tori with minimal energy. In particular, the two $\mathbb{T}^2$ parametrised by $\mathcal{L}_\pm$ have the same energy. Outside of $\mathcal{L}_\pm$ the surface $\mathcal{B}$ parametrises a single family of $\mathbb{T}^2$. To the side of $\mathcal{L}_\pm$ 'covered' by $\mathcal{F}_0$ this is $\mathbb{T}^2_A(v)$ and to the sides 'covered' by $\mathcal{F}_\pm$ this is $\mathbb{T}^2_B(v)$. In a similar way, when passing through $(0, \ell^*, 0)$ the $\mathbb{T}^2$-family surrounding the normal 3-mode is $\mathbb{T}^2_A(v)$, while $\mathbb{T}^2_B(v)$ consists of 2-tori even for critical values $v = (\mu, \ell, h)$ with $\mu = 0$. At the cusp value the two families $\mathbb{T}^2_A(v)$ and $\mathbb{T}^2_B(v)$, $v \in \mathcal{L}_+$ (or $v \in \mathcal{L}_-$) coincide with the hyperbolic $\mathbb{T}^2$ parametrised by $\mathcal{F}_h$ as the figure eight yielding the stable=unstable manifolds of the latter has shrunk to a point.

To better understand the placement of $\mathcal{T}''$ with respect to the rest of $\mathcal{C}$ and, in particular, to $\mathcal{B}$, consider the straight line $\mathcal{C}_{12}$ with $(\mu, \ell, h) = (0, \ell, 0)$, $\ell < 0$. Then place the tetrahedral structure in such a way that the edge between $\mathcal{F}_+$ and $\mathcal{F}_-$ is a subset of $\mathcal{C}_{12}$ and does not extend to the origin (where all C_{ij} meet). The edges $\mathcal{L}_\pm$ should then be glued to $\mathcal{B}$ while being distinct from $\mathcal{C}_{13}$ and $\mathcal{C}_{23}$, which also belong to $\mathcal{B}$. Note that $\mathcal{B}$ is not smooth along $\mathcal{L}_\pm$, along $\mathcal{C}_{13}$ and $\mathcal{C}_{23}$, and along the part of $\mathcal{C}_{12}$ that belongs on $\mathcal{B}$. The lack of smoothness along $\mathcal{L}_\pm$ and $\mathcal{C}_{13,23}$ allows $\mathcal{T}''$ to be glued with $\mathcal{B}$ in the indicated way.

In fact, locally around $\mathcal{L}_+$ it seems better to view the surfaces not as part of $\mathcal{B}$ and $\mathcal{T}''$, but as two smooth surfaces parametrising $\mathbb{T}^2_A(v)$ and $\mathbb{T}^2_B(v)$, respectively, that intersect along $\mathcal{L}_+$ (similar for $\mathcal{L}_-$). In the same way, the surface parametrising $\mathbb{T}^2_B(v)$ is pierced through by $\mathcal{C}_{12}$, at $(0, \ell^*, 0)$ the short line $(\mu, \ell, h) = (0, \ell, 0)$ does not detach smoothly.

Remark 15. Again the transitional case $\delta = 1$ helps to explain the structure of the set $\mathcal{C}$ of critical values. When passing through $\delta = 1$ the tetrahedral surface $\mathcal{T}''$ with its non-empty intersection with $\mathcal{B}$ shrinks down to a single value where $\mathcal{C}_{12}$ detaches from $\mathcal{B}$. At $\delta = 1$ this value corresponds to a degenerate Hamiltonian Hopf bifurcation and the set $\mathcal{C}$ of critical values already looks like the one depicted in Fig. 15. Note that this does not indicate a different type of degenerate Hamiltonian Hopf bifurcation — strongly 'tilted' planes have the same kind of transition when passing through one of the other two degenerate Hamiltonian Hopf bifurcations.

Case $\mathbf{1 < \delta}$. For large positive detuning $\delta > 1$ the intersection of the plane $\lambda = \delta$ with the amended bifurcation diagram attains its simplest form, see Fig. 15(left). The intersection consists only of the straight half line $\mu = 0$, $\ell \le -\lambda^2$, which starts at a supercritical Hamiltonian Hopf bifurcation and extends indefinitely.

The set $\mathcal{C}$ of critical values depicted in Fig. 15(right) consists of the surface $\mathcal{B}$ where values lift to $\mathbb{T}^2$, except along the curves $\mathcal{C}_{ij}$, $ij = 12, 13, 23$. In particular, critical values along $\mathrm{int}(\mathcal{C}_{ij} \cap \mathcal{B})$, $ij = 12, 13, 23$ (dashed lines in Fig. 15) correspond to stable normal modes and where these three meet we have the elliptic equilibrium. Critical values on $\mathcal{C}^0_{12} = \mathcal{C}^+_{12}$ (the half line $(0, \ell, 0)$, $\ell < -\lambda^2$) correspond to the Cartesian product of a $\mathbb{T}^1$ (the normal 3-mode) and a pinched torus (its stable=unstable manifold). The normal 3-mode loses its stability in a supercritical Hamiltonian Hopf bifurcation where the half line $\mathcal{C}_{12}$ detaches from $\mathcal{B}$ to become $\mathcal{C}^0_{12} = \mathcal{C}^+_{12}$.

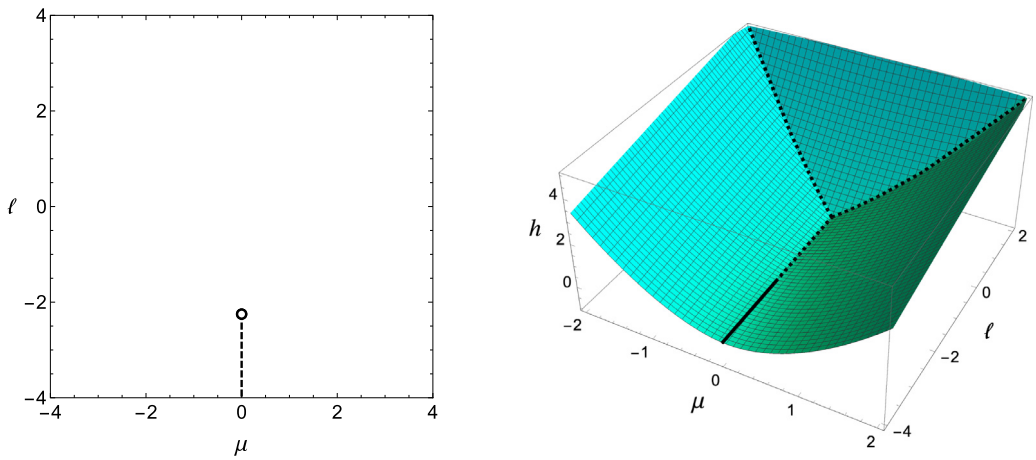

Fig. 15. Intersection of the plane $\lambda = 1.5$ with the amended bifurcation diagram and the corresponding set of critical values $\mathcal{C}$.

Remark 16. For $\kappa = 0$ the fibres of the energy–momentum mapping need not be compact. Correspondingly, not only the cases with $\delta \geq \frac{1}{2}$ are lost, but also the interpretation for small detuning $\delta < \frac{1}{2}$ (i.e. the passage through $\delta = 0$) changes. What remains are the tetrahedral sets $\mathcal{T}$ and $\mathcal{T}'$ shrinking down to the origin $(\mu, \ell, h) = (0, 0, 0)$ as $\delta \nearrow 0$ and $\delta \searrow 0$, respectively. Regular values $v \in \mathcal{R}''$ parametrise $\mathbb{T}^3_B(v)$ that shrink down to elliptic $\mathbb{T}^2_B(v)$, $v \in \mathcal{F}^\circ_e$ surrounding the three normal modes and to hyperbolic $\mathbb{T}^2_B(v)$, $v \in \mathcal{F}_h$ which at $\mathcal{D}'$ meet the elliptic $\mathbb{T}^2$ in quasi-periodic centre-saddle bifurcations. When passing through the 1:1:−2 resonance, $\mathcal{T}$ shrinks down to the origin and re-emerges as $\mathcal{T}'$ flipped upside-down.

In comparison to this, the 'final stage' $\delta > 1$ depicted in Fig. 15 also has three faces of $\mathcal{B}$ parametrising elliptic $\mathbb{T}^2$, but the 'hyperbolic face' has vanished along with two of the subcritical Hamiltonian Hopf bifurcations, while the third Hamiltonian Hopf bifurcation has become supercritical. In particular, $\kappa \neq 0$ provides not only for compact level sets $\mathbb{T}^3_A(v)$, v a regular value of $\mathcal{EM}$, but also for critical values with minimal energy (maximal energy if $\kappa < 0$). When $\kappa = 0$ higher order terms in the normal form (19) are needed to decide what other invariant sets are parametrised by regular values of $\mathcal{EM}$ inside and outside of $\mathcal{T}$ and $\mathcal{T}'$.

5. Monodromy

In this section we determine the monodromy for the system defined by the normalised Hamiltonian $H^\delta_{N,L}$ given in (19). We briefly recall some basic facts about monodromy in integrable Hamiltonian systems as they apply to the system under study here.

Consider a closed path γ in the set $\mathcal{R}$ of regular values of the energy–momentum mapping $\mathcal{EM}$. Then $\mathcal{EM}^{-1}(\gamma)$ is a, possibly non-trivial, $\mathbb{T}^3$-fibre bundle over γ. The non-triviality of the bundle can be expressed through the glueing mapping $\psi : \mathbb{T}^3 \longrightarrow \mathbb{T}^3$ of the bundle over the circle γ. The mapping ψ induces a mapping ψ_* on $H_1(\mathbb{T}^3) \simeq \mathbb{Z}^3$ which, fixing a basis of $H_1(\mathbb{T}^3)$, can be written as a matrix of $\mathrm{SL}(3, \mathbb{Z})$ which is called the *monodromy matrix* of the bundle. The monodromy matrix depends only on the homotopy class $[\gamma]$ of a path γ in $\mathcal{R}$ and we thus denote the monodromy matrix by $M_{[\gamma]}$. The mapping

$$M \;:\; \pi_1(\mathcal{R}) \;\longrightarrow\; \mathrm{SL}(3, \mathbb{Z})$$

that assigns to each homotopy class $[\gamma]$ of $\mathcal{R}$ the corresponding monodromy matrix $M_{[\gamma]}$ is called the *monodromy mapping* of the system.

Note that not the energy–momentum mapping $\mathcal{EM}$ itself, but its set $\mathcal{R}$ of regular values is the main ingredient of the monodromy mapping M. This allows us to use any diffeomorphism of $\mathbb{R}^3$ to transform $\mathcal{R}$ into a form suitable for our considerations; in particular we may use any of the alternatives of $\mathcal{EM} = (N, L, H^\delta_{N,L})$ discussed at the beginning of Section 4. Thus, we again replace $H^\delta_{N,L}$ by $\mathcal{H}_\lambda$ as defined in (21) but considered as a function $\mathcal{H}_\lambda : \mathbb{R}^6 \longrightarrow \mathbb{R}$ and now also replace L by $J = \frac{1}{2}(N + L)$, i.e. we work with

$$\mathcal{EM} \;=\; (N, J, \mathcal{H}_\lambda)$$

where λ depends on the values μ of N and ι of J through

$$\lambda \;=\; \delta \;+\; (\lambda_1 - \lambda_2)\mu \;+\; 2\lambda_2\iota$$

which replaces (20). Because of the existence of the effective global $\mathbb{T}^2$-action Φ generated by X_N and X_J, we choose as a basis for expressing the monodromy matrix a basis of $H_1(\mathbb{T}^3) \simeq \mathbb{Z}^3$ given by the homology cycles g_N, g_J represented by

periodic orbits of X_N and X_J on $\mathbb{T}^3$ and completed by any other homology cycle g with the property that (g_N, g_J, g) form a basis.

Remark 17. The reason we need to consider here the effective action generated by X_N and X_J, rather than the non-effective action generated by X_N and X_L, manifests here. The cycles g_N and g_L generated by the flows of X_N and X_L cannot be combined with any other cycle to form a basis of $H_1(\mathbb{T}^3)$. In particular, g_J cannot be expressed as an integer linear combination of g_N and g_L, since the definition of J implies $g_L + g_N = 2g_J$.

Then the monodromy matrix for $[\gamma]$ can be written in such basis as

$$M_{[\gamma]} \;=\; \begin{pmatrix} 1 & 0 & m_N^{[\gamma]} \\ 0 & 1 & m_J^{[\gamma]} \\ 0 & 0 & 1 \end{pmatrix} \;.$$

The given monodromy matrix signifies that parallel transport of g_N and g_J along γ gives g_N and g_J respectively, while parallel transport of g gives $g + m_N^{[\gamma]} g_N + m_J^{[\gamma]} g_J$.

Remark 18. The cycle g completing the basis (g_N, g_J, g) is not uniquely determined: any cycle $g' = g + k_N g_N + k_J g_J$ also defines a basis of $H_1(\mathbb{T}^3)$ with the same orientation. However, different choices of g do not affect the monodromy matrix since, if g is parallel transported along γ to some cycle $\hat{g} = g + m_N^{[\gamma]} g_N + m_J^{[\gamma]} g_J$, then g' is parallel transported to $\hat{g}' = g' + m_N^{[\gamma]} g_N + m_J^{[\gamma]} g_J$ (because g_N and g_J do *not* change under parallel transport).

We define the *monodromy vector* for $[\gamma]$ by

$$\vec{m}^{[\gamma]} \;=\; (m_N^{[\gamma]}, m_J^{[\gamma]}) \;\in\; \mathbb{Z}^2 \;.$$

The mapping

$$\vec{m} \;=\; (m_N, m_J) \;\mapsto\; M(\vec{m}) \;=\; \begin{pmatrix} 1 & 0 & m_N \\ 0 & 1 & m_J \\ 0 & 0 & 1 \end{pmatrix}$$

exhibits a group isomorphism between $(\mathbb{Z}^2, +, \vec{0})$ and the subgroup of $(\mathrm{SL}(3,\mathbb{Z}), \cdot, I)$ that is the image of $\pi_1(\mathcal{R})$ under the monodromy mapping. In particular,

$$M(\vec{0}) \;=\; I \;,\quad M(\vec{m}_1)M(\vec{m}_2) \;=\; M(\vec{m}_1 + \vec{m}_2) \;,\quad M(\vec{m})^{-1} \;=\; M(-\vec{m}) \;.$$

Therefore, the existence of the global $\mathbb{T}^2$-action Φ implies that, even though $\pi_1(\mathcal{R})$ may not be abelian, its image under the monodromy mapping is an abelian subgroup of $\mathrm{SL}(3,\mathbb{Z})$. Note that if $\pi_1(\mathcal{R})$ is generated by k not necessarily commuting paths $[\gamma_1], \ldots, [\gamma_k]$, then we can expand

$$[\gamma] \;=\; \prod_{j=1}^{K} \prod_{i=1}^{k} [\gamma_i]^{a_{i,j}}$$

into K factors, i.e. with $\sum_{i=1}^{k} a_{i,j} = 1$, $j = 1, \ldots, K$ and the corresponding monodromy vector $\vec{m}^{[\gamma]}$ is given by

$$\vec{m}^{[\gamma]} \;=\; \sum_{i=1}^{k} a_i \vec{m}^{[\gamma_i]} \;,$$

where $a_i = \sum_{j=1}^{K} a_{i,j}$. It is therefore sufficient to compute the monodromy vector for the generators of $\pi_1(\mathcal{R})$. We do this computation in Section 5.1 using the approach of [12].

5.1. Computation of monodromy

We compute monodromy for the cases for which the sets $\mathcal{C}$ of critical values were described in Section 4.2. Recall that the system has always three curves of critical values parametrising the three normal modes $\mathcal{C}_{23}$, $\mathcal{C}_{13}$ and $\mathcal{C}_{12}$. The monodromy of the ramified torus bundle defined by the energy–momentum mapping $\mathcal{EM}$ is largely determined by these three curves and whether parts of them are transversally isolated in the image of $\mathcal{EM}$ or whether they are embedded in some two-dimensional surface $\mathcal{B}$ of critical values. These two possibilities also largely determine $\pi_1(\mathcal{R})$. In all cases considered in Section 4.2, the fundamental group $\pi_1(\mathcal{R})$ is non-trivial although its structure is not always the same. Moreover, in some cases monodromy can be meaningfully defined for loops γ that contain critical values of $\mathcal{EM}$, see [11] for more details.

Remark 19. The monodromy of a similar n-degree-of-freedom Hamiltonian system where n threads of critical values join at the origin has been studied in [13, Example 1.2]. The monodromy of that system is determined using a convenient representation where monodromy acts trivially to $n-2$ cycles generating the $\mathbb{T}^n$-fibre homology.

5.1.1. Case $\delta = \lambda_1 = \lambda_2 = 0$

We first determine the monodromy mapping for the resonant system without detuning, cf. Section 4.2.1. Part of this computation has been given in [12], with the exception of an overall "sign" of the monodromy vector (which depends on a careful choice of orientations and was outside the scope of [12]). In this case $\pi_1(\mathcal{R})$ is isomorphic to the free product $\mathbb{Z}*\mathbb{Z}$ and is generated by two closed paths: one path $[\gamma_1]$ encircling the thread $\mathcal{C}^0_{23}$ and one path $[\gamma_2]$ encircling the thread $\mathcal{C}^0_{13}$. The threads $\mathcal{C}^0_{23}$ and $\mathcal{C}^0_{13}$ are oriented so that they start at infinity and point to the origin. Then the paths $[\gamma_1]$ and $[\gamma_2]$ are oriented so that they follow the right-hand rule with respect to $\mathcal{C}^0_{23}$ and $\mathcal{C}^0_{13}$, respectively. Note that $[\gamma_1]$ and $[\gamma_2]$ do not commute. We further define $[\gamma_3] = [\gamma_1]^{-1} \cdot [\gamma_2]^{-1}$. Such a homotopy class is represented by a path that encircles $\mathcal{C}^0_{12}$. Following the same orientation conventions, $[\gamma_3]$ is positively oriented. Since $[\gamma_1] \cdot [\gamma_2] \cdot [\gamma_3] = 1$ we conclude that

$$\vec{m}^{[\gamma_1]} + \vec{m}^{[\gamma_2]} + \vec{m}^{[\gamma_3]} = \vec{0} \ . \tag{47}$$

Given equation (47), we here first compute $\vec{m}^{[\gamma_2]}$ and $\vec{m}^{[\gamma_3]}$, from which we then deduce $\vec{m}^{[\gamma_1]}$.

To compute $\vec{m}^{[\gamma_2]}$ we consider a specific representative of $[\gamma_2]$ on a plane $N = \mu < 0$. Using $(J, \mathcal{H}_\lambda)$ as co-ordinates on the plane $N = \mu < 0$, the thread $\mathcal{C}^0_{13}$ intersects the plane at $(J, \mathcal{H}_\lambda) = (0, \frac{1}{2}\mu^2) =: c_2$. Then $[\gamma_2]$ can be represented by a circle C_2 that winds once counterclockwise around c_2 with respect to the oriented co-ordinates $(J, \mathcal{H}_\lambda)$ on the $N = \mu < 0$ plane and which bounds a disk U_2 on this plane. The disk U_2 contains one Φ-orbit with non-trivial isotropy $\mathbb{T}^1_J$ generated by X_J. Following [12] we note that in the basis (X_N, X_J) we can write $X_J = (0, 1)$ and therefore the corresponding monodromy vector should be $\vec{m}^{[\gamma_2]} = \pm(0, 1)$, where the sign must be determined. For a positively oriented (counterclockwise) path on the oriented $(J, \mathcal{H}_\lambda)$-plane the sign is $+1$ if the Φ-orbit with non-trivial isotropy is *positive* in the sense of [12] and is -1 otherwise. The $\mathbb{T}^1_J$-action acts on the reduced space

$$N^{-1}(\mu < 0)/\!\!/_{\mathbb{T}^1_N} \simeq \mathbb{C}^2$$

(where $\mathbb{T}^1_N$ is generated by X_N) as

$$(z_1 z_2, z_3) \mapsto (\mathrm{e}^{2\pi i t} z_1 z_2, \mathrm{e}^{-2\pi i t} z_3) \ ,$$

with complex co-ordinates $z_1 z_2$ and z_3 on $N^{-1}(\mu < 0)/\mathbb{T}^1_N$. We note here that the two co-ordinates $z_1 z_2$ and z_3 define an orientation that coincides with the one induced by symplectic reduction. Since $\mathbb{T}^1_J$ has weights 1:0:-1 the Φ-orbit is positive (it would have been negative if the weights were 1:0:1) and we conclude that

$$\vec{m}^{[\gamma_2]} = (0, 1) \ .$$

We can repeat the same argument to compute $\vec{m}^{[\gamma_3]}$. The isotropy in this case is $\mathbb{T}^1_N$ and in the basis (X_N, X_J) we have $\vec{m}^{[\gamma_3]} = \pm(1, 0)$. The $\mathbb{T}^1_N$-action on the reduced space $J^{-1}(\iota < 0)/\mathbb{T}^1_J$ reads as

$$(z_1 z_3, z_2) \mapsto (\mathrm{e}^{2\pi i t} z_1 z_3, \mathrm{e}^{-2\pi i t} z_2)$$

whence the corresponding Φ-orbit is again positive. The only difference is that $[\gamma_3]$ is now represented by a negatively oriented (clockwise) circle C_3 on the plane $J = \iota < 0$. Therefore

$$\vec{m}^{[\gamma_3]} = (-1, 0)$$

and with (47) finally

$$\vec{m}^{[\gamma_1]} = (1, -1) \ .$$

Note that in these computations of the monodromy vectors the specific form of the Hamiltonian $\mathcal{H}_\lambda$ is not used. This implies that in subsequent cases, where the parameters of the Hamiltonian change, the monodromy vectors remain the same for paths $[\gamma_k]$, $k = 1, 2, 3$, provided that such paths can be defined (see Section 5.1.3).

5.1.2. Case $\delta < 0$, $\lambda_1 = \lambda_2 = 0$

In this case $\mathcal{R}$ consists of two connected components: one outside $\mathcal{T}$ denoted $\mathcal{R}'$, and one inside $\mathcal{T}$ denoted $\mathcal{R}''$. The fundamental group $\pi_1(\mathcal{R}')$ is isomorphic to $\mathbb{Z} * \mathbb{Z}$ and the whole discussion from the previous subsection can be transferred almost verbatim here. Indeed, for closed paths in $\mathcal{R}'$ the tetrahedral surface $\mathcal{T}$ together with its interior $\mathcal{R}''$ is indistinguishable from the mere point value $(\mu, \iota, h) = (0, 0, 0)$ where the three threads meet when $\delta = \lambda_1 = \lambda_2 = 0$. The fundamental group $\pi_1(\mathcal{R}'')$ is trivial and thus its image under the monodromy mapping is the identity.

However, monodromy is also meaningful [11] for paths γ that do not lie completely in $\mathcal{R}'$ or $\mathcal{R}''$, but pass from one connected component to the other through $\mathcal{F}^\circ_e$. Then $\mathcal{EM}^{-1}(\gamma)$ is the disjoint union of a $\mathbb{T}^3$-bundle for which we can define monodromy and another manifold that can be ignored. We use this to extend the monodromy mapping M to $\pi_1(\mathcal{R}^+)$, where $\mathcal{R}^+$ contains both the interior and the exterior of $\mathcal{T}$, but not the face $\mathcal{F}_h$ of $\mathcal{T}$. In this extension the 'ignorable' manifold does not contribute to M, reflecting that $\pi_1(\mathcal{R}'')$ is trivial. For example, if γ enters and exits $\mathcal{R}''$ through the same face $\mathcal{F}_{0,\pm}$, then we can reduce the whole $\mathbb{T}^2$-action Φ; the family $\mathbb{T}^3_B(v)$ becomes a cylinder $\mathbb{T}^1_B(v)$ shrinking to points at the two values $v \in \mathcal{F}_{0,\pm}$, revealing the reduced ignorable manifold to be $\mathbb{S}^2$ and the ignorable manifold itself to be diffeomorphic to $\mathbb{S}^2 \times \mathbb{T}^2$. If γ enters and exits $\mathcal{R}''$ once through different faces of $\mathcal{F}^\circ_e$, then only a $\mathbb{T}^1$-subaction of Φ

can be regularly reduced (the normal mode 'between' the two faces of $\mathcal{F}_e^\circ$ having non-trivial isotropy) and the relevant $\mathbb{T}^2_B(v)$ shrink to $\mathbb{T}^1_B(v)$, $v \in \mathcal{F}_e^\circ$ forming an $\mathbb{S}^3$; the ignorable manifold is diffeomorphic to $\mathbb{S}^3 \times \mathbb{T}^1$.

Note that we may also consider paths γ that pass through one of the parts of the $\mathcal{C}_{ij}$ that form the common topological boundaries of the $\mathcal{F}_{0,\pm}$. Indeed, while this may allow for e.g. a deformation of $\mathbb{S}^2 \times \mathbb{T}^2$ into $\mathbb{S}^3 \times \mathbb{T}^1$, this manifold is then ignored anyway.

We therefore let $\mathcal{R}^+ := \mathcal{R} \cup \mathcal{F}_e$ and define a monodromy mapping $M : \pi_1(\mathcal{R}^+) \longrightarrow \mathrm{SL}(3,\mathbb{Z})$ by considering only the monodromy of the $\mathbb{T}^3$-bundle connected component of $\mathcal{EM}^{-1}(\gamma)$ for γ in $\mathcal{R}^+$. The fundamental group $\pi_1(\mathcal{R}^+)$ is isomorphic to $\pi_1(\mathcal{R})$ and is also generated by the same paths $[\gamma_1]$ and $[\gamma_2]$ for which we found in Section 5.1.1 that $\vec{m}^{[\gamma_1]} = (1,-1)$ and $\vec{m}^{[\gamma_2]} = (0,1)$. Therefore, the results for the monodromy mapping $\pi_1(\mathcal{R}) \longrightarrow \mathrm{SL}(3,\mathbb{Z})$ for the case $\delta = \lambda_1 = \lambda_2 = 0$ apply without any further modifications to determine the monodromy mapping $M : \pi_1(\mathcal{R}^+) \longrightarrow \mathrm{SL}(3,\mathbb{Z})$. The extension of M from $\pi_1(\mathcal{R}')$ to $\pi_1(\mathcal{R}^+)$ means that we may interpret the three threads (which meet at the single value $(\mu,\iota,h) = (0,0,0)$ for $\delta = \lambda_1 = \lambda_2 = 0$) as meeting at $\mathcal{F}_h$ instead of meeting at $\mathcal{T} \cup \mathcal{R}''$.

5.1.3. Case $\delta > 0$, $\lambda_1 = \lambda_2 = 0$

Following the structure of the discussion in Section 4.2.3, we again distinguish the three cases of small, intermediate and large positive detuning separated by $\delta = \frac{1}{2}$ and $\delta = 1$.

Case $\mathbf{0 < \delta < \frac{1}{2}}$. This case is exactly the same as the case $\delta < 0$. We again define $\mathcal{R}^+ = \mathcal{R} \cup \mathcal{F}_e$ with the only difference being that now $\mathcal{F}_e$ is the "lower" part of $\mathcal{T}'$. The fundamental group $\pi_1(\mathcal{R}^+)$ remains isomorphic to $\mathbb{Z} * \mathbb{Z}$ and the rest of the discussion goes through without any other changes.

Case $\mathbf{\frac{1}{2} < \delta < 1}$. Here the set of regular values consists again of two connected components $\mathcal{R}'$ and $\mathcal{R}''$ which are, respectively, outside and inside $\mathcal{T}''$. However, there are two important changes here with respect to previous cases. First, $\pi_1(\mathcal{R}')$ is isomorphic to $\mathbb{Z}$. It is generated by $[\gamma_3]$ which winds once around the thread of critical values $\mathcal{C}_{12}$ and for which we computed in Section 5.1.1 that the monodromy vector is $\vec{m}^{[\gamma_3]} = (-1,0)$.

Second, we can no longer consider paths that enter $\mathcal{R}''$ through one of the sides $\mathcal{F}_\pm$ and exit through $\mathcal{F}_0$ or vice versa. For such paths γ, the pre-image $\mathcal{EM}^{-1}(\gamma)$ does not contain a $\mathbb{T}^3$-bundle over a circle and therefore we cannot define monodromy. However, we can still consider paths that enter and exit $\mathcal{R}''$ through the union of $\mathcal{F}_+$ and $\mathcal{F}_-$ with their common topological boundary, and paths that both enter and exit $\mathcal{R}''$ through $\mathcal{F}_0$. Recall that the topological boundary of $\mathcal{F}_0$ consists of the common boundary with $\mathcal{F}_h$ and the two curve segments $\mathcal{L}_\pm$ on $\mathcal{B}$. The space of such paths together with paths that lie entirely in $\mathcal{R}'$ or $\mathcal{R}''$ is generated by $[\gamma_3]$ and therefore the corresponding homotopy structure is isomorphic to $\mathbb{Z}$.

Case $\mathbf{1 < \delta}$. In this case $\pi_1(\mathcal{R})$ is isomorphic to $\mathbb{Z}$ and generated by $[\gamma_3]$. The monodromy then is completely determined by the monodromy vector $\vec{m}^{[\gamma_3]} = (-1,0)$. One may think of the passage of δ through $\delta = 1$ from $\delta > 1$ to $\delta < 1$ as replacing the value $(\delta, 0, -\delta^2)$, $\delta > 1$ by $\mathcal{F}_h \cup \mathcal{L}_\pm$ conditional on paths γ not encircling $\mathcal{L}_+$ or $\mathcal{L}_-$ (i.e. paths that enter the interior $\mathcal{R}''$ of $\mathcal{T}''$ through $\mathcal{F}_0$ exit $\mathcal{R}''$ through $\mathcal{F}_0$ as well).

5.2. Global monodromy

Letting the detuning parameter $\delta = \lambda$ (i.e. $\lambda_1 = \lambda_2 = 0$) vary we may consider $\mathcal{EM} = (N, J, \mathcal{H}_\lambda)$ as a mapping

$$\begin{array}{ccc} \mathbb{R}^6 \times \mathbb{R}^1 & \longrightarrow & \mathbb{R}^3 \times \mathbb{R}^1 \\ (q,p,\lambda) & \mapsto & (\mu,\iota,h,\lambda) \end{array},$$

thereby stacking all δ-values together to let the parametrised sets of critical values form a single subset of $\mathbb{R}^4$. This results in a single monodromy mapping assembling the δ-family of monodromy mappings.

Remark 20. This approach is less theoretical than it seems since in applications the detuning parameter δ may easily arise as the value of some additional action D, see Section 6.

6. Conclusions

An integrable[1] Hamiltonian system in three degrees of freedom with an equilibrium in 1:1:−2 resonance, has a set $\mathcal{C}$ of critical values of the energy–momentum mapping $\mathcal{EM} = (N, L, H^0_{N,L})$ of the normal form (19) depicted in Fig. 9, with three threads parametrising unstable normal modes meeting at the value of the equilibrium. This results in a monodromy mapping

$$\mathbb{Z} * \mathbb{Z} \longrightarrow \mathrm{SL}(3,\mathbb{Z}) \tag{48}$$

[1] Admitting both the axial symmetry generated by the third component N of the angular momentum and the oscillator symmetry generated by the quadratic part L of the Hamiltonian.

with commutative image isomorphic to $\mathbb{Z}^2$ spanned by the monodromy vectors $\vec{m}^{[\gamma_1]} = (1, -1)$ and $\vec{m}^{[\gamma_2]} = (0, 1)$. A small amount of detuning leaves (48) unchangend, but stabilises the detuned resonant equilibrium and with it the three normal modes, deforming the set $\mathcal{C}$ of critical values of $\mathcal{EM}$ into those depicted in Fig. 10 and 12 and thereby turning the monodromy into island monodromy. For large detuning, depending on the relative size (and sign) of third and 4th order terms in the normal form (19), the monodromy mapping becomes

$$\mathbb{Z} \longrightarrow \mathrm{SL}(3, \mathbb{Z}) \tag{49}$$

with $\pi_1(\mathcal{R})$ generated by a loop around the single thread in Fig. 15. The mapping (49) describes the (island) monodromy already for intermediate values of the detuning where the set $\mathcal{C}$ of critical values of $\mathcal{EM}$ has the more complicated form depicted in Fig. 13. As discussed in [6,21] monodromy remains meaningful for the non-integrable Hamiltonian (5) approximated by the integrable normal form (19) and persists even under small perturbations that destroy the axial symmetry. However, for the latter perturbations the non-degeneracy conditions mentioned in Remark 9 that exclude low order normal-internal resonances become important.

Our choice to retain in the normal form (19) next to the third order term X also the terms of order 4 had the dynamical consequence that all motions remained bounded – mostly spinning densely around invariant 3-tori – but furthermore turned the bifurcation diagram of Fig. 5 into the one depicted in Fig. 3. This resulted in additional bifurcations – compare Table 4 with Table 3 – which lead to the different type (49) of monodromy for large and intermediate detuning. To actually prove that the phenomena discovered in a normal form can also be observed in the original system one often uses a scaling that zooms in on smaller and smaller neighbourhoods of the equilibrium. In the present situation this would make the 4th order terms smaller and smaller and correspondingly already intermediate detuning larger and larger, see (22). In the similar situation of periodic orbits in normal-internal resonance the semi-global approach in [14] to the 1:3 resonance reveals the hyperbolic 3-periodic orbit that causes the transitional instability of the initial periodic orbit at the 1:3 resonance to undergo a periodic centre-saddle bifurcation for a parameter value nearby the 1:3 resonance; a phenomenon observed in many applications. We therefore expect that also the cusp and supercritical Hamiltonian Hopf bifurcations emanating from the degenerate Hamiltonian Hopf bifurcations do accompany 1:1:−2 resonances where these occur.

In order to interpret the 'external' detuning as an internal parameter one can study periodic orbits in four degrees of freedom instead of equilibria in three degrees of freedom. Indeed, while the latter are generically isolated the former form 1-parameter families, parametrised by the action D conjugate to the angle along the periodic orbit (for non-zero Floquet exponents one may even parametrise by the energy). Let us impose axial symmetry and assume that the Floquet exponents encounter a 1:1:−2 resonance. Then it is generic for the value δ of D to detune the resonance. Normalising with respect to the periodic motion – possible under non-degeneracy conditions that exclude normal-internal resonances between the normal frequencies and the period – then allows to reduce the $\mathbb{T}^1$-action generated by D with reduced Hamiltonian in three degrees of freedom of the form (5). See also Remark 20 in Section 5.2.

One should keep in mind that even in axially symmetric Hamiltonian systems it is *not* generic for the 1-parameter families of periodic orbits to encounter a normal 1:1:−2 resonance. The reason is that adding βN to (5) detunes the 1:1 subresonance, see Remark 3. To account for this second parameter one could study invariant 2-tori (with their two actions D and B conjugate to the toral angles acting as two internal parameters) in an integrable system of five degrees of freedom and then reduce the $\mathbb{T}^2$-symmetry along the $\mathbb{T}^2$-tori to three degrees of freedom, resulting in a (relative) equilibrium in 1:1:−2 resonance. However, when breaking the symmetries of the integrable system (the above $\mathbb{T}^2$-symmetry, the $\mathbb{T}^1$-symmetry generated by L and the axial symmetry generated by N) the 2-parameter family of invariant 2-tori needs KAM theory to persist and a single torus in normal 1:1:−2 resonance may disappear in a resonance gap (opened by the necessary Diophantine conditions on the two internal frequencies).

It is only in six (or more) degrees of freedom that families of invariant lower dimensional tori with three (or more) internal frequencies may encounter a normal n_1:n_2:n_3 resonance in such a way that the normally resonant tori even after perturbation away from integrability form a non-empty Cantor family parametrised by a Cantor set of dimension one (or more). In this way the detuning does become one of the internal parameters and the phenomena of the previous sections do persistently occur in six or more degrees of freedom. For the 1:1:−2 resonance the occurrence co-dimension increases because of the 1:1 subresonance, again see Remark 3, and one needs at least eight degrees of freedom. The non-integrable 1:1:−2 resonance, just like its definite counterpart, is a rather degenerate phenomenon.

Acknowledgements

A.M. was supported by INdAM (Istituto Nazionale di Alta Matematica "F. Severi") and by the Grant Agency of the Czech Republic, project 17-11805S.

Appendix. Proof of Proposition 11

While the proposition is formulated for $\kappa = 1$, the value actually used in Figs. 3 and 4 and in Table 3, we give the proof here for general $\kappa \neq 0$ to provide for complete formulas. Lemma 10 allows us to compute the bifurcation diagram of the system via the triple roots of $F(R)$ that lie in $[R_{\min}, \infty[$. We obtain such roots by factorising $F(R)$ as

$$F(R) = \frac{\kappa^2}{4}(R - a)^3(R - b) , \tag{50}$$

where a is the sought out triple root and $b \in \mathbb{R}$ is the remaining root of $F(R)$. Comparing coefficients of powers of R in the two expressions (33) and (50) for $F(R)$ we obtain the relations

$$\begin{aligned} -\kappa^2 a^3 b + 4h^2 - 4\mu^2 \ell &= 0 && (51a)\\ \kappa^2 a^3 + 3\kappa^2 a^2 b - 8h\lambda + 4\mu^2 &= 0 && (51b)\\ -3\kappa^2 a^2 - 3\kappa^2 ab - 4\kappa h + 4\lambda^2 + 4\ell &= 0 && (51c)\\ 3\kappa^2 a + \kappa^2 b + 4\kappa\lambda - 4 &= 0\ . && (51d) \end{aligned}$$

Solving (51b)–(51d) for b, ℓ and h we find

$$\begin{aligned} b &= 4\kappa^{-2} - 3a - 4\kappa^{-1}\lambda && (52a)\\ 2\lambda\ell &= -2\kappa^3 a^3 - 6\kappa^2 a^2\lambda + 3\kappa a^2 - 6\kappa a\lambda^2 + 6a\lambda - 2\lambda^3 + \kappa\mu^2 && (52b)\\ 2\lambda h &= \mu^2 + 3a^2 - 2\kappa^2 a^3 - 3\,\kappa a^2\lambda && (52c) \end{aligned}$$

which for $\lambda \neq 0$ yields an explicit parametrisation by λ and a. The remaining equation (51a) becomes

$$\frac{1}{\lambda^2} Q(\mu) = 0\ ,$$

where

$$\begin{aligned} Q(\mu) = {} & (1 - 2\kappa\lambda)\,\mu^4 \\ & + \left(4\kappa^3 a^3\lambda - 4\kappa^2 a^3 + 12\kappa^2 a^2\lambda^2 - 12\kappa a^2\lambda + 6a^2 + 12\kappa a\lambda^3 - 12a\lambda^2 + 4\lambda^4\right)\mu^2 \\ & + \left(4\kappa^4 a^6 + 12\kappa^3 a^5\lambda - 12\kappa^2 a^5 + 12\kappa^2 a^4\lambda^2 - 18\kappa a^4\lambda + 9a^4 + 4\kappa a^3\lambda^3 - 4a^3\lambda^2\right) \end{aligned}$$

is quadratic in μ^2 for $\lambda \neq \frac{1}{2\kappa}$.

This makes $\lambda = \frac{1}{2\kappa}$ a special case, next to $\lambda = 0$. Below we shall first check these two special cases before treating the general cases $\lambda < 0$, $0 < \lambda < \frac{1}{2\kappa}$ and $\lambda > \frac{1}{2\kappa}$.

More degenerate than a triple root of F is having a quadruple root, i.e. $b = a$ in (50). From (52a) then follows

$$a = \frac{1}{\kappa^2} - \frac{\lambda}{\kappa}\ . \qquad (53)$$

As (33) is a polynomial of degree 4 we have $F^{(4)} \equiv 6\kappa^2$ and in particular $F^{(4)}(a) \neq 0$ — the quadruple root (53) is not of order 5 or higher. In Section 3.4 we have seen that for $a = R_{\min}$ this yields the degenerate Hamiltonian Hopf bifurcations at

$$(\lambda, \mu, \ell) = \left(\frac{1}{2\kappa}, \frac{\pm 1}{2\kappa^2}, \frac{1}{2\kappa^2}\right) \quad \text{and} \quad (\lambda, \mu, \ell) = \left(\frac{1}{\kappa}, 0, \frac{-1}{\kappa^2}\right)$$

and from Lemma 10 we conclude that for $a > R_{\min}$ this yields cusp bifurcations.

A.1. Special cases

We first check the special cases $\lambda = 0$ and $\lambda = \frac{1}{2\kappa}$.

Case $\boldsymbol{\lambda = 0}$. Setting $\lambda = 0$ in (52) gives

$$b = \frac{4}{\kappa^2} - 3a \quad \text{and} \quad \mu^2 = (2\kappa^2 a - 3)a^2\ .$$

Inserting this in (51) we obtain the quadratic equation

$$\ell^2 + \left(-2\kappa^4 a^3 + 6\kappa^2 a^2 - 6a\right)\ell + \left(3\kappa^4 a^4 - 10\kappa^2 a^3 + 9a^2\right) = 0 \qquad (54)$$

in ℓ with discriminant $a^3(\kappa^2 a - 2)^3$. The condition $a \geq R_{\min} \geq |\mu|$ implies $a^2 \geq \mu^2$ and $a \geq 0$, and gives

$$a^2(2 - \kappa^2 a) \geq 0\ ,$$

that is $0 \leq a \leq 2\kappa^{-2}$. For these values (54) has negative discriminant and thus non-real roots except for the end points $a = 0$ and $a = 2\kappa^{-2}$ of the interval. For $a = 0$ we find $\mu = \ell = a = 0$, recovering the equilibrium in 1:1:−2 resonance with values $(\lambda, \mu, \ell) = (0, 0, 0)$. While this is what makes $\lambda = 0$ special, for $a = 2\kappa^{-2}$ we find $\pm\mu = \ell = a = 2\kappa^{-2}$, corresponding to a supercritical Hamiltonian Hopf bifurcation. These are not special, but belong to the 1-parameter families of supercritical Hamiltonian Hopf bifurcations $\mathbf{HH}_1^+$ and $\mathbf{HH}_2^+$, see below.

Case $\boldsymbol{\lambda = \frac{1}{2\kappa}}$. Here the equation $Q(\mu) = 0$ becomes linear in μ^2 and in particular it factorises to

$$(2\kappa^2 a - 1)^3(\mu^2 - 2\kappa^2 a^3) \;=\; 0$$

whence $a = \frac{1}{2\kappa^2}$ or $\mu^2 = 2\kappa^2 a^3$. Where both equations are satisfied we recover the two degenerate Hamiltonian Hopf bifurcations $\mathbf{HH}_1^0$ and $\mathbf{HH}_2^0$. For $a = \frac{1}{2\kappa^2}$ we have

$$b \;=\; \frac{1}{2\kappa^2} \;=\; a \;, \quad \ell \;=\; \frac{1}{4\kappa^2} + \kappa^2\mu^2 \quad \text{and} \quad h \;=\; \frac{1}{8\kappa^3} + \kappa\mu^2$$

where the parametrisation of ℓ and h by μ is restricted by $|\mu| \le \frac{1}{2\kappa^2}$, as obtained from $a \ge R_{\min} \ge \max(|\mu|, \ell)$. Therefore

$$(\lambda, \mu, \ell) \;=\; \left(\frac{1}{2\kappa},\, \mu,\, \frac{1}{4\kappa^2} + \kappa^2\mu^2\right) \;, \quad |\mu| \;\le\; \frac{1}{2\kappa^2}$$

parametrises a 1-parameter family of cusp bifurcations that we denote by $\mathbf{CB}_3$ and which extends between $\mathbf{HH}_1^0$ and $\mathbf{HH}_2^0$. While this is what makes $\lambda = \frac{1}{2\kappa}$ special, for $\mu^2 = 2\kappa^2 a^3$ we have

$$b \;=\; -3a + \frac{2}{\kappa^2} \;, \quad \ell \;=\; \frac{6\kappa^2 a - 1}{4\kappa^2} \quad \text{and} \quad h \;=\; \frac{3\kappa a^2}{2} \;.$$

Since $a^2 \ge \mu^2 = 2\kappa^2 a^3$ and $a \ge 0$ we find $0 \le a \le \frac{1}{2\kappa^2}$ (the second inequality also following from $a \ge \ell$) where $a = \pm\mu$ gives the end points $a = 0$ and $a = \frac{1}{2\kappa^2}$. We have already seen that the right end point $a = \frac{1}{2\kappa^2}$ yields the two degenerate Hamiltonian Hopf bifurcations $\mathbf{HH}_1^0$ and $\mathbf{HH}_2^0$. The left end point $a = 0$ yields $(\lambda, \mu, \ell) = (\frac{1}{2\kappa}, 0, \frac{-1}{4\kappa^2})$ which belongs to the family $\mathbf{HH}_3^-$ of subcritical Hamiltonian Hopf bifurcations, see below. In between the parametrisation

$$(\lambda, \mu, \ell) \;=\; \left(\frac{1}{2\kappa},\, \pm\sqrt{2\kappa^2 a^3},\, \frac{6\kappa^2 a - 1}{4\kappa^2}\right) \;, \quad 0 \;<\; a \;<\; \frac{1}{2\kappa^2}$$

yields centre-saddle bifurcations which turn out to belong to the 2-parameter families of centre-saddle bifurcations $\mathbf{CS}_1$ and $\mathbf{CS}_2$, see again below.

A.2. General case: $\boldsymbol{\lambda \neq 0,\ \frac{1}{2\kappa}}$

Solving the quadratic equation $Q(\mu) = 0$ for μ^2 we find the two solutions

$$\mu_\pm^2 = \frac{\pm 2|\lambda|}{2\kappa\lambda - 1}\left[(\kappa a + \lambda)^2 - 2a\right]^{3/2} + \frac{2\kappa^3 a^3\lambda - 2\kappa^2 a^3 + 6\kappa^2 a^2\lambda^2 - 6\kappa a^2\lambda + 3a^2 + 6\kappa a\lambda^3 - 6a\lambda^2 + 2\lambda^4}{2\kappa\lambda - 1} \tag{55a}$$

and

$$2\lambda\ell_\pm \;=\; -2\kappa^3 a^3 \;-\; 6\kappa^2 a^2\lambda \;+\; 3\kappa a^2 \;-\; 6\kappa a\lambda^2 \;+\; 6a\lambda \;-\; 2\lambda^3 \;+\; \kappa\mu_\pm^2 \;. \tag{55b}$$

These solutions are real provided that the discriminant $16\lambda^2[(\kappa a + \lambda)^2 - 2a]^3$ of $Q(\mu)$, the latter seen as a quadratic polynomial in μ^2, is non-negative. While this is always true for $\lambda > \frac{1}{2\kappa}$, this gives for $\lambda < \frac{1}{2\kappa}$ the sub-cases

$$0 \;\le\; \kappa^2 a \;\le\; 1 - \kappa\lambda - \sqrt{1 - 2\kappa\lambda} \quad \text{and} \quad \kappa^2 a \;\ge\; 1 - \kappa\lambda + \sqrt{1 - 2\kappa\lambda} \;.$$

Case $\boldsymbol{\lambda > \frac{1}{2\kappa}}$. Here, the condition $a \ge \ell_+$ is not satisfied for any $a \ge 0$. Therefore, the solutions μ_+, ℓ_+ in (50) can be rejected.

We have checked with Mathematica that the condition $a \ge \ell_-$ is satisfied for all $a \ge 0$ and that $a^2 \ge \mu_-^2$ is also true. We note that the condition $\mu_-^2 \ge 0$ gives

$$a\,g(a) \;\le\; 0$$

with

$$g(a) \;=\; 4\kappa^4 a^3 \;+\; \left(12\kappa^3\lambda - 12\kappa^2\right)a^2 \;+\; \left(12\kappa^2\lambda^2 - 18\kappa\lambda + 9\right)a \;+\; \left(4\kappa\lambda^3 - 4\lambda^2\right) \;. \tag{56}$$

For $a = 0$ the inequality $a\,g(a) \le 0$ is satisfied for any value of $g(a)$. If $a > 0$ then we require that $g(a) \le 0$ and check that $g(0) = 4\kappa^2\lambda^2(\kappa\lambda - 1)$ and that $g(a)$ has two extrema at strictly negative values of a. This means that for $\frac{1}{2\kappa} < \lambda < \frac{1}{\kappa}$ the cubic equation $g(a) = 0$ has a unique positive root $a_0(\lambda)$ and thus $g(a) \le 0$ for $0 \le a \le a_0(\lambda)$. This yields centre-saddle bifurcations at the triple roots $a > R_{\min}$ while for $\kappa^2 a = 1 - \kappa\lambda$ we have $b = a$ and get cusp bifurcations (recall that the non-degeneracy condition $F^{(4)}(a) \neq 0$ is always true in our system).

We have $0 \le 1 - \kappa\lambda \le \kappa^2 a_0(\lambda)$, therefore the bifurcations are split to several 2-parameter families of centre-saddle bifurcations separated by cusp bifurcations. The centre-saddle bifurcations are the family $\mathbf{CS}_4$ parametrised by

$$\frac{1}{2\kappa} < \lambda < \frac{1}{\kappa}\ , \quad \mu = \pm\mu_-\ , \quad \ell = \ell_-\ , \quad 1 - \kappa\lambda < \kappa^2 a < \kappa^2 a_0(\lambda)\ .$$

Then, a part of the family $\mathbf{CS}_1$ is parametrised by

$$\frac{1}{2\kappa} < \lambda < \frac{1}{\kappa}\ , \quad \mu = \mu_-\ , \quad \ell = \ell_-\ , \quad 0 < \kappa^2 a < 1 - \kappa\lambda$$

and a part of $\mathbf{CS}_2$ is parametrised by

$$\frac{1}{2\kappa} < \lambda < \frac{1}{\kappa}\ , \quad \mu = -\mu_-\ , \quad \ell = \ell_-\ , \quad 0 < \kappa^2 a < 1 - \kappa\lambda\ .$$

There are two families of cusp bifurcations denoted by $\mathbf{CB}_1$ and $\mathbf{CB}_2$. They can be obtained from $\mathbf{CS}_4$ by setting $\kappa^2 a = 1 - \kappa\lambda$. This gives for $\mathbf{CB}_1$ that

$$\frac{1}{2\kappa} < \lambda < \frac{1}{\kappa}\ , \quad \mu = \mu_- = \kappa^{-2}(\kappa\lambda - \sqrt{2\kappa\lambda - 1})\ , \quad \ell_- = 1 - \kappa\lambda - \sqrt{2\kappa\lambda - 1}$$

and for $\mathbf{CB}_2$ the same parametrisation up to $\mu = -\mu_-$.

For $\lambda \ge \kappa^{-1}$ we have $g(a) > 0$ for all $a > 0$ and therefore the only possibility that is left is $a = 0$. Subsequently, for $\lambda \ge \kappa^{-1}$, we obtain by substituting $a = 0$ that

$$\mu_\pm^2 = 0 \quad \text{and} \quad \ell_\pm = -\lambda^2\ .$$

So, for $\lambda > \kappa^{-1}$ we have the family of supercritical Hamiltonian Hopf bifurcations parametrised by $(\lambda, \mu, \ell) = (\lambda, 0, -\lambda^2)$ and denoted by $\mathbf{HH}_3^+$. This can be checked using the derivative $F'''(a = 0) = 6(\kappa\lambda - 1) > 0$.

Case $\boldsymbol{\lambda < \frac{1}{2\kappa}}$, $\boldsymbol{\lambda \neq 0}$. The condition $a \ge \ell_-$, together with $a \ge 0$ and $a^2 \ge \mu_-^2 \ge 0$, gives

$$\kappa^2 a \ \ge\ 1 - \kappa\lambda + \sqrt{1 - 2\kappa\lambda}$$

or

$$\kappa^2 a_0(\lambda) \ \le\ \kappa^2 a \ \le\ 1 - \kappa\lambda - \sqrt{1 - 2\kappa\lambda}\ , \quad \lambda < 0$$

and

$$0 \ \le\ \kappa^2 a \ \le\ 1 - \kappa\lambda - \sqrt{1 - 2\kappa\lambda}\ , \quad \lambda > 0\ .$$

Here $a_0(\lambda)$ is the unique real root of (56). This parametrises the part of the family $\mathbf{CS}_1$ with $\lambda < \frac{1}{2}$ for $\mu = \mu_-$ and the corresponding part of $\mathbf{CS}_2$ for $\mu = -\mu_-$. The condition $a \ge \ell_+$, together with $a \ge 0$ and $a^2 \ge \mu_+^2 \ge 0$, gives

$$\kappa^2 a \ \ge\ 1 - \kappa\lambda + \sqrt{1 - 2\kappa\lambda}$$

or

$$0 \ \le\ \kappa^2 a \ \le\ 1 - \kappa\lambda - \sqrt{1 - 2\kappa\lambda}\ , \quad \lambda < 0$$

and

$$\kappa^2 a_0(\lambda) \ \le\ \kappa^2 a \ \le\ 1 - \kappa\lambda - \sqrt{1 - 2\kappa\lambda}\ , \quad \lambda > 0\ .$$

This parametrises the family $\mathbf{CS}_3$ for $\mu = \pm\mu_+$. Note that for $\kappa^2 a = 1 - \kappa\lambda - \sqrt{1 - 2\kappa\lambda}$ we have $\mu_+^2 = \mu_-^2 = a^2$ and $\ell_+ = \ell_- = a$. Therefore we obtain two curves parametrising subcritical Hamiltonian Hopf bifurcations since here $F'''(a) = -6\sqrt{1 - 2\kappa\lambda} < 0$. The two curves are $\mathbf{HH}_1^-$ and $\mathbf{HH}_2^-$. For $\kappa^2 a = 1 - \kappa\lambda + \sqrt{1 - 2\kappa\lambda}$ we obtain the two curves

$$\ell = a\ , \quad \mu = \pm a\ , \quad \lambda = \pm\sqrt{2a} - \kappa a\ , \quad a \ge 0$$

which can alternatively be written as

$$\ell = \kappa^{-2}(1 - \kappa\lambda + \sqrt{1 - 2\kappa\lambda})\ , \quad \mu = \pm\ell\ , \quad \lambda < \frac{1}{2\kappa}\ .$$

These two curves parametrise families of supercritical Hamiltonian Hopf bifurcations since here $F'''(a) = 6\sqrt{1 - 2\kappa\lambda} > 0$. The curves are $\mathbf{HH}_1^+$ and $\mathbf{HH}_2^+$.

Note that for $\lambda = 0$ these expressions give $\ell = 2\kappa^{-2}$, $\mu = \pm 2\kappa^{-2}$ which are two of the values we already identified for $\lambda = 0$. Considering now the constraint $0 \leq \kappa^2 a \leq 1 - \kappa\lambda - \sqrt{1 - 2\kappa\lambda}$ for $\lambda = 0$ we find $a = 0$ and thus $\ell = \mu = 0$. This is the third value we identified for $\lambda = 0$. Therefore, we can extend the parametrisation for $\lambda < \frac{1}{2\kappa}$ to include the case $\lambda = 0$.

References

[1] R. Abraham, J.E. Marsden, Foundations of Mechanics, 2nd ed., Benjamin, 1978.
[2] V.I. Arnol'd, V.V. Kozlov, A.I. Neishtadt, Mathematical aspects of classical and celestial mechanics, in: V.I. Arnol'd (Ed.), Dynamical Systems III, Springer, 1988.
[3] M.L. Bertotti, Localization of closed orbits of nonlinear Hamiltonian systems with 1, −2 resonance near an equilibrium, Boll. Unione Mat. Ital.(7) 1-B (1987) 965–978.
[4] T.J. Bridges, Bifurcation of periodic solutions near a collision of eigenvalues of opposite signature, Math. Proc. Cambridge Philos. Soc. 108 (1990) 575–601.
[5] T.J. Bridges, Stability of periodic solutions near a collision of eigenvalues of opposite signature, Math. Proc. Cambridge Philos. Soc. 109 (1991) 375–403.
[6] H.W. Broer, R.H. Cushman, F. Fassò, F. Takens, Geometry of KAM tori for nearly integrable Hamiltonian systems, Ergodic Theory Dynam. Systems 27 (2007) 725–741.
[7] O. Christov, Non-integrability of first order resonances of Hamiltonian systems in three degrees of freedom, Celestial Mech. Dynam. Astronom. 112 (2012) 147–167.
[8] R.H. Cushman, L.M. Bates, Global Aspects of Classical Integrable Systems, Birkhäuser, 1997.
[9] G.F. Dell'Antonio, B.M. D'Onofrio, On the number of periodic solutions of an Hamiltonian system near an equilibrium point, Boll. Unione Mat. Ital.(6) 3B (1984) 809–835.
[10] J.J. Duistermaat, Non-integrability of the 1:1:2-resonance, Ergodic Theory Dynam. Systems 4 (1984) 553–568.
[11] K. Efstathiou, H.W. Broer, Uncovering fractional monodromy, Comm. Math. Phys. 324 (2013) 549–588.
[12] K. Efstathiou, N. Martynchuk, Monodromy of Hamiltonian systems with complexity 1 torus actions, J. Geom. Phys. 115 (2017) 104–115.
[13] M. Gross, Special Lagrangian fibrations. I. Topology, in: M.-H. Saito, Y. Shimizu, K. Ueno (Eds.), Integrable Systems and Algebraic Geometry, Kobe/Kyoto 1997, World Scientific, 1998, pp. 156–193.
[14] H. Hanßmann, Local and Semi–Local Bifurcations in Hamiltonian Dynamical Systems — Results and Examples, LNM, vol. 1893, Springer, 2007.
[15] H. Hanßmann, I. Hoveijn, The 1: 1 resonance in Hamiltonian systems, J. Differential Equations 266 (11) (2018) 6963–6984.
[16] H. Hanßmann, J.C. van der Meer, On the Hamiltonian Hopf bifurcations in the 3*D* Hénon–Heiles family, J. Dynam. Differential Equations 14 (2002) 675–695.
[17] H. Hanßmann, J.C. van der Meer, Algebraic methods for determining Hamiltonian Hopf bifurcations in three-degree-of-freedom systems, J. Dynam. Differential Equations 17 (3) (2005) 453–474.
[18] J.N. Mather, Differentiable invariants, Topology 16 (1977) 145–155.
[19] J.C. van der Meer, Degenerate Hamiltonian Hopf bifurcations, in: L.M. Bates, D.L. Rod (Eds.), Conservative systems and quantum chaos, Waterloo 1992, Fields Institute Communications, vol. 8, AMS, 1996, pp. 159–176.
[20] J.C. van der Meer, The Hamiltonian Hopf bifurcation, LNM, vol. 1160, Springer, 1985.
[21] B. Rink, A Cantor set of tori with monodromy near a focus-focus singularity, Nonlinearity 17 (2004) 347–356.
[22] D.A. Sadovskiĭ, B.I. Zhilinskiĭ, Hamiltonian systems with detuned 1:1:2 resonance: manifestation of bidromy, Ann. Physics 322 (2007) 164–200.
[23] J.A. Sanders, F. Verhulst, J. Murdock, Averaging Methods in Nonlinear Dynamical Systems, second edition, Appl. Math. Sci., vol. 59, Springer, 2007.
[24] G.W. Schwarz, Smooth functions invariant under the action of a compact Lie group, Topology 14 (1975) 63–68.